結果が得られた。また、多重加工をアデノウイルス（1元）、PEI（2元）、コンドロイチン硫酸（3元）、以降PEIとコンドロイチン硫酸を順次加えていき、7元まで検討したところ、8元以降においてアデノウイルス-LacZの感染性が増加し、腫瘍溶解性アデノウイルスの高い抗腫瘍効果が得られた。走査型電子顕微鏡的検討により、立体的構造を検討した。溶媒について比較検討したところ、PBS、HEPES、Tris等の電解質を使用すると、固定後に多量の結晶が認められたため、5%グルコース液を用いることとした。静置による加工では、1元では単一分子であるものの、2元以降のウイルスのほとんどが凝集していた。この凝集を抑制するため、rotator（回転装置）、ミキサー（タイター テック社）による検討を行ったところ、rotatorでは凝集の改善は全く認められず、ミキサーのslow、fastの2段階撹拌においてfastのうち5段階中3段階目の速度で10分間ミキシングすると、最も良好な抗体存在下における感染性と、走査型電子顕微鏡観察下での凝集が抑制できることが明らかとなった。（図1）

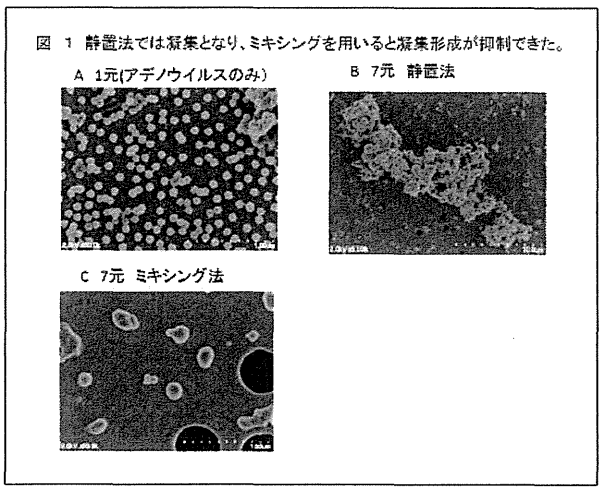

ポリマー加工アデノウイルスの標的癌細胞への感染効率をさらに改善するため、強い陽性荷電を有するPEIに比べ生体由来物質で弱い陰性荷電を有するコンドロイチン硫酸より、さらに強力な陰性荷電を有するヘパリンを用いて、PEIの陽性荷電を中和し血清蛋白との結合を防ぎ、次の実験を行った。13元処理後にヘパリン処理を行ったところ、抗体存在下においてFCS非存在下で3時間反応後、FCSを加えると、13元処理に比べ3倍ほどの感染が認められた。しかしながら、最初からFCSおよび抗体を加えるとその感染性はFCS非存在下での実験に比べ30%程度減少した。これは、ヘパリンの本来有しているFCS中の血液凝固因子とその他の蛋白質との結合によるものと思われた。このため、腫瘍特異性を有するEGFをさらに加えると、FCS存在下、非存在下において感染性と抗腫瘍効果の増大が認められた。（図2）

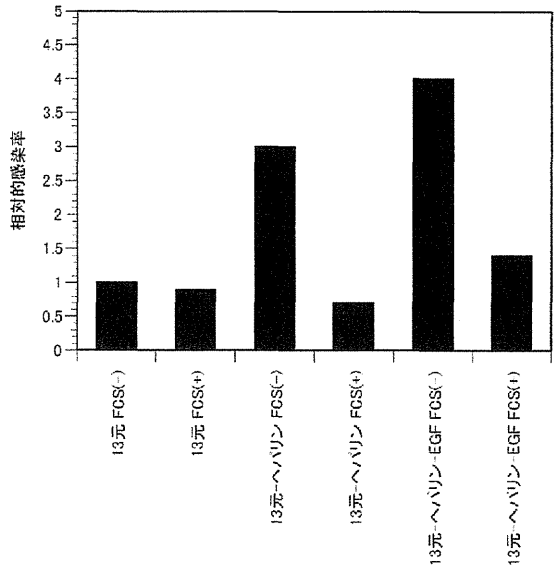

ウイルスを用いた毒性試験が可能な施設は極めて少ないため、その実験条件を検討する必要がある。このため、イヌを用いて、腫瘍溶解性アデノウイルスに対する毒性試験の予備試験を行った。皮下投与後、血中中和抗体価は上昇するものの、血液、糞便、尿、唾液、摘出臓器において、プラーク形成ユニット（PFU） アッセイおよびリアルタイム定量的DNA-PCRにより、腫瘍溶解性アデノウイルスは検出されなかった。また、第二クール目以降のイヌにおいて、腫瘍溶解性アデノウイルス投与前に既に抗体価の上昇が認められ、注射部位からの腫瘍溶解性アデノウイルスの漏出の可能性が疑われるため、創部の感染予防の管理と実験終了後には、UVあるいは滅菌消毒（エタノール、次亜塩素酸処理）による十分な部屋のクリーンアップが必要と思われた。

D. 考察

腫瘍溶解性アデノウイルスのポリマー加工による抗体による感染抑制解除には、室温で、ミキサーを用いた十分な攪拌条件の下で加工することが必要であることが明らかとなった。従来、ポリマー加工後のプラスミドあるいはウイルスに関しては、局所投与においては十分な抗腫瘍効果が認められるものの、静脈内投与においては投与後の急死が問題であったが、今回の検討により、これは、静置処理によるウイルスの凝集が原因であることが明らかとなった。この凝集は、ミキシングによる攪拌での加工により防ぐことができ、粒子径の小さい単一分子での加工が可能となり、安全に静脈内投与が可能になるものと思われる。PEIとコンドロイチン硫酸によるポリマー加工に加えて、ヘパリンさらにはEGF等の成長因子による加工により感染性の改善が望めるのみなら

ず、成長因子による腫瘍特異的感染性の向上も望める可能性が示唆され、今後、成長因子の選択が重要課題になってくるものを思われる。

ヒト臨床試験のための毒性試験において、イヌ正常線維芽細胞における in vitro MV-NPL 感染実験の結果から、実験動物としてサルの他に、イヌが適応する可能性が示唆された。腫瘍溶解性アデノウイルスによる予備的毒性試験の結果から、血中抗体価の測定、注射部位の感染源としての管理と実験犬相互の感染防止、実験終了後の部屋のクリーンアップ等が重要になるものと思われた。また、伴侶動物医薬品市場の成長が著しいものがあり、こうした分野におけるMV-NPLのポリマー加工製品が癌治療薬として認可され、さらにヒト医薬品へのトランスレーションすることにより、より閉塞状況にある国内の医薬品開発が容易となる新たなビジネスモデルになる可能性が示唆された。

E. 結論

腫瘍溶解性アデノウイルスのポリマー加工には、室温でミキシング処理が感染力向上につながり、ヘパリン、成長因子の追加加工によりより効果的な治療システムが構築でき、同様にMV-NPLにおいても同様な加工により効果的治療システムの構築が可能になるものと思われる。

F. 健康危険情報

特になし

G. 研究発表

1. 論文発表

1.Yoshihara, C., Hamada, K., Kuroda, M. and Koyama, Y. Oncolytic plasmid: A novel strategy for tumor immuno-gene therapy. Oncology Letters 3:387-390. 2012

2. Hamada, K., Yoshihara, C., Ito, T., Tani, K., Tagawa, M., Sakuragawa, N., Itoh, H. and Koyama, Y. Antitumor effect of chondroitin sulfate-coated ternary GM-CSF plasmid complex for ovarian cancer. Journal of Gene Medicine, 14: 120–127.2012

3. Hiwasa, K., Nagaya, H., Terao, S., Acharya, B., Hamada, K., Mizuguchi, H. and Gotoh, A. Improved gene transfer into bladder cancer cells using adenovirus vector containing RGD motif. Anticancer research 32:3137-3140.2012

2. 学会発表

1. Hamada, K., Yoshihara, C., Ito, T., Koyama, Y., Itoh, H., Takagi, K., Nawa, A. Gene therapy of chondroitin sulfate-coated ternary GM-CSF plasmid complex for ovarian cancer. American Society of Gene & Cell Therapy 15th Annual Meeting. Philadelphia, Pennsylvania May 15, 2012 - May 19, 2012.

2. 濱田雄行、高木香津子、芳原智恵子、小山義之、那波明宏. ポリマー多重加工処理によるオンコリティックアデノウイルスの免疫原性克服と抗腫瘍効果の検討. 第71回日本癌学会、2012年9月19-21日、札幌

H. 知的財産権の出願・登録状況

（予定を含む。）

1. 特許取得

特になし

2. 実用新案登録

特になし

3. その他

特になし

研究成果の刊行に関する一覧表

書籍

著者氏名	論文タイトル名	書籍全体の編集者名	書　籍　名	出版社名	出版地	出版年	ページ
谷憲三朗	GM-CSFによる樹状細胞発達の調節	高久　史麿	血液内科	科学評論社	東京都	2012	873-880

雑誌

発表者氏名	論文タイトル名	発表誌名	巻号	ページ	出版年
Yokota, Y., Inoue, H., Matsumura, Y., Nabeta, H., Narusawa, M., Watanabe, A., Sakamoto, C., Hijikata, Y., Iga-Murahashi, M., Takayama,K., Sasaki, F., Nakanishi, Y., Yokomizo, T.,Tani, K..	Absence of LTB4/BLT1 axis facilitates generation of mouse GM-CSF-induced long-lasting antitumor immunological memory by enhancing innate and adaptive immune systems	Blood	120	3444-3543	2012
Miyamoto,S., Inoue , H., Nakamura ,T., Yamada , M., Sakamoto , C., Urata , Y., Okazaki, T., Marumoto, T., Takahashi, A., Takayama,K., Nakanishi, Y., Shimizu, H., Tani,K	Coxsackievirus B3 Is an oncolytic virus with immunostimulatory properties that is active against lung adenocarcinoma	Cancer Res	72	2609-2621	2012
Mizuochi, C., Hirio, Y., BIasch,K., Kikushige,Y., Tani,K., Akashi,K., Tavian,M., Sugiyama, D.	Intra-aortic clusters undergo endothelial to hematopoietic phenotypic changes in early embryogenesis.	PLoS ONE	7	e35763	2012
Dong, Y., Kobayashi, S., Tian, Y., Ozawa, M., Hiramoto, T., Izawa, K., Bai,Y., Soda, Y., Sasaki, E., Itoh, T., Maru, Y., Oyaizu, N., Tojo, A., Kai, C., Tani, K.	Leukemogenic fusion gene (p190 BCR-ABL) transduction into hematopoietic stem/progenitor cells in the common marmoset	Open J Blood Dis	2	1-10	2012
Somada,S., Muta, H., Nakamura,K., Sun,X., Honda,K., Ihara, E.,Akiho, H., Takayanagi, R., Yoshikai, Y., Podack, E.R., Tani, K.	CD30 Ligand/CD30 Interaction is involved in pathogenesis of inflammatory bowel disease	Dig Dis Sci	57	2031-2037	2012

Nunomura,S., Shimada,S., Kametani,Y., Yamada,Y., Yoshioka,M., Suemizu,H., Ozawa,M., Itoh ,T., Kono ,A., Suzuki, R., Tani, K., Ando, K., Yagita, H., Ra, C., Habu, S., Satake, M., Sasaki, E.	Double expression of CD34 and CD117 on bone marrow progenitors is a hallmark of the development of functional mast cell of Callithrix jacchus (common marmoset).	Int Immunol	24	593-603	2012
Yoshihara,C.,Hamada,K.,Kuroda.M.,Koyama,Y.	Oncolytic plasmid:A novel strategy for tumor immuno-gene therapy	ONCOLOGY LETTERS	3	387-390	2012
Hiwasa.K.,Nagaya.H.,Terao,S.,Acharya.B.,Hamada,K.,Mizoguchi,H.,Gotoh,A.,	Improved gene transfer into bladder cancer cells using adenovirus vector containing RGD motif	ANTICANCER RESEARCH	32	3137-3140	2012
Hamada,K., Yoshihara, C., Ito, T., Tani,K., Tagawa, M., Sakuragawa,N., Ito, H.,Koyama, Y.	Antitumor effect of chondroitin sulfate-coated ternary granulocyte macrophage colony-stimulating factor plasmid complex for ovarian cancer.	J Gene Med.	14	5120-5127	2012
Liao,J.,Marumoto,T., Yamaguchi,S., Okano,S.,Takeda, N.,Sakamoto,C., Kawano,H.,Nii,T., Miyamoto, S., Nagai, Y., Okada, M., Inoue, H.,Kawahara,K., Suzuki, A., Miura, Y., Tani K	Inhibition of PTEN tumor suppressor promotes the generation of induced pluripotent stem cells.	Mol Ther	-	in press	2013
Kurita,R.,Suda,N., Sudo,K.,Miharada,K.,Hiroyama,T.,Miyoshi,H.,Tani,K., Nakamura,Y.	Establishment of immortalized human erythroid progenitor cell lines able to produce enucleated red blood cells	PLoS ONE	-	in press	2013
Hiramoto,T.,Ebihara, Y.,Mizoguchi,Y., Nakamura,K.,Yamauchi,K.,Ueno,K., Nariai,N.,Mochizuki, S.,Yamamoto, .,Nagasaki, M., Furukawa, Y.,Tani,K.,Nakauchi, H., Kobayashi, M., Tsuji, K,	Wnt3a stimulates maturation of impaired neutrophils developed from severe congenital neutropenia patient-derived pluripotent stem cells	Proc Natl Acad Sci USA	110	3023-3028	2013

Absence of LTB4/BLT1 axis facilitates generation of mouse GM-CSF–induced long-lasting antitumor immunologic memory by enhancing innate and adaptive immune systems

*Yosuke Yokota,[1] *Hiroyuki Inoue,[1-3] Yumiko Matsumura,[1] Haruka Nabeta,[1] Megumi Narusawa,[1] Ayumi Watanabe,[1] Chika Sakamoto,[1] Yasuki Hijikata,[3] Mutsunori Iga-Murahashi,[3] Koichi Takayama,[2] Fumiyuki Sasaki,[4] Yoichi Nakanishi,[2] Takehiko Yokomizo,[4] and Kenzaburo Tani[1,3]

[1]Department of Molecular Genetics, Medical Institute of Bioregulation, Kyushu University, Fukuoka, Japan; [2]Research Institute for Diseases of the Chest, Graduate School of Medical Sciences, Kyushu University, Fukuoka, Japan; [3]Department of Advanced Cell and Molecular Therapy, Kyushu University Hospital, Kyushu University, Fukuoka, Japan; and [4]Department of Medical Biochemistry, Graduate School of Medical Sciences, Kyushu University, Fukuoka, Japan

BLT1 is a high-affinity receptor for leukotriene B4 (LTB4) that is a potent lipid chemoattractant for myeloid leukocytes. The role of LTB4/BLT1 axis in tumor immunology, including cytokine-based tumor vaccine, however, remains unknown. We here demonstrated that BLT1-deficient mice rejected subcutaneous tumor challenge of GM-CSF gene-transduced WEHI3B (WGM) leukemia cells (KO/WGM) and elicited robust antitumor responses against second tumor challenge with WEHI3B cells. During GM-CSF–induced tumor regression, the defective LTB4/BLT1 signaling significantly reduced tumor-infiltrating myeloid-derived suppressor cells, increased the maturation status of dendritic cells in tumor tissues, enhanced their CD4$^+$ T-cell stimulation capacity and migration rate of dendritic cells that had phagocytosed tumor-associated antigens into tumor-draining lymph nodes, suggesting a positive impact on GM-CSF–sensitized innate immunity. Furthermore, KO/WGM mice displayed activated adaptive immunity by attenuating regulatory CD4$^+$ T subsets and increasing numbers of Th17 and memory CD44^{hi}CD4$^+$ T subsets, both of which elicited superior antitumor effects as evidenced by adoptive cell transfer. In vivo depletion assays also revealed that CD4$^+$ T cells were the main effectors of the persistent antitumor immunity. Our data collectively underscore a negative role of LTB4/BLT1 signaling in effective generation and maintenance of GM-CSF–induced antitumor memory CD4$^+$ T cells. (*Blood.* 2012;120(17):3444-3454)

Introduction

For many cancers refractory to conventional therapies, gene-modified tumor vaccines have emerged as a promising treatment. Among numerous immunostimulatory cytokines used for tumor vaccines, GM-CSF has been the most intensively investigated and widely studied for use in clinical cancer vaccine trials.[1-3] Immunization with irradiated tumor cells engineered to secrete GM-CSF stimulates potent tumor-associated antigen (TAA)-specific antitumor immunity in preclinical[4,5] and clinical settings, including solid tumors and acute myeloid leukemia.[6,7] We have recently shown that the GM-CSF gene-transduced murine monocytic leukemia of WEHI3B cells lose their tumorigenicity when subcutaneously administered into wild-type (WT) BALB/c mice.[8] It is thought that the effective induction of antitumor immunity triggered by GM-CSF is mainly the result of augmented processing and presentation of TAAs by dendritic cells (DCs), followed by both CD4$^+$ and CD8$^+$ T-cell responses.[4,9,10] However, the efficacy of this therapy alone is not durable, partially because of its failure to maintain antitumor memory immunity by TAA-primed T cells. Therefore, there is an imminent need for elaborate studies to improve antitumor memory responses generated by GM-CSF gene-transduced tumor cells.

Leukotriene B4 (LTB4) is known to be an extremely potent lipid inflammatory mediator derived from membrane phospholipids by the sequential actions of 5-lipoxygenase and LTA4 hydrolase.[11] The major activities of LTB4 include the recruitment and activation of myeloid leukocytes, such as neutrophils.[12] Recently, Del Prete et al have reported a novel role of LTB4 in regulating migration of DCs that precede adaptive immune responses.[13] Lipid LTB4 mediates its functions through the G protein-coupled 7 transmembrane domain receptor superfamily,[14] namely, 2 distinct receptors, BLT1 and BLT2. On the other hand, GM-CSF stimulates the production and function of neutrophils, eosinophils, and monocytes, and activate maturation of DCs.[15,16] However, the underlying significance of the LTB4/BLT1 lipid chemo-attractant pathway in the field of tumor immunology, including GM-CSF-induced immunity, remains elusive.

In this context, we investigated the influence of the defective LTB4/BLT1 axis on antitumor memory responses induced by subcutaneous administration of WGM cells using WT and BLT1-knockout (KO) mice. Intriguingly, in vivo experiments showed that marked tumor rejection was reproduced only in BLT1-KO mice when WEHI3B cells were subcutaneously inoculated into WT or BLT1-KO mice that had rejected the outgrowth of WGM cells, implying that that the loss of the LTB4/BLT1 signaling may confer effective generation of TAA-specific memory T cells with retained antitumor effects triggered by GM-CSF. Therefore, the current

Submitted October 5, 2011; accepted August 13, 2012. Prepublished online as *Blood* First Edition paper, August 30, 2012; DOI 10.1182/blood-2011-10-383240.

*Y.Y. and H.I. contributed equally to this study.

The online version of this article contains a data supplement.

The publication costs of this article were defrayed in part by page charge payment. Therefore, and solely to indicate this fact, this article is hereby marked "advertisement" in accordance with 18 USC section 1734.

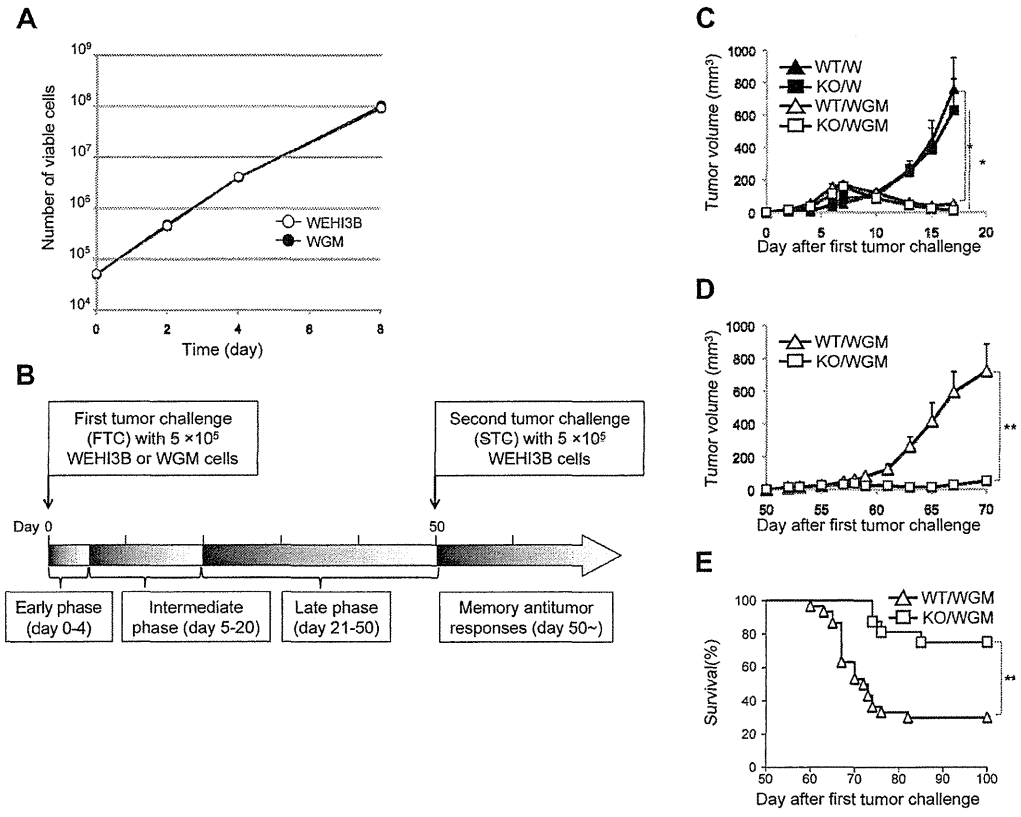

Figure 1. The absence of LTB4/BLT1 signaling induces potent antitumor effects against the second tumor challenge of WEHI3B cells after marked regression of WGM cells in mice model. (A) WEHI3B and WGM cells were cultured separately at 1×10^4 cells/well for 2, 4, 6, and 8 days in CM. At each time point, the number of viable cells was determined by trypan blue dye exclusion assay. (B) The explanatory scheme for all of the following in vivo experiments. The early phase, intermediate phase, and late phase in tumorigenicity assay are defined as spanning from days 0-4, 5-20, and 21-50 after the FTC, respectively. (C) In vivo tumorigenicity assay. The FTC consisted of 5×10^5 WEHI3B or WGM cells subcutaneously inoculated into the right flank of WT or BLT1-KO mice (n = 6–8). (D-E) In vivo STC assay. On day 50 after the FTC, 5×10^5 WEHI3B cells were subcutaneously inoculated into the left flank of mice that completely rejected the challenged tumor cells. The tumor volumes (mm^3) in 4 indicated mice groups were assessed on day 17. Kaplan-Meier survival curves are shown after the STC. Bars represent mean ± SEM. Significant difference: $^*P < .05$, $^{**}P < .01$. Representative data from 2-6 independent experiments with similar results are shown.

study explored the role of the LTB4/BLT1 signaling pathway in the induction of the persistent GM-CSF–induced antitumor memory responses.

Methods

Mice

BLT1-KO mice were established using a gene-targeting strategy, as previously described.[17] BLT1-KO mice and the corresponding WT mice have been backcrossed onto a BALB/c genetic background > 10 times. All animal experiments were carried out under the Guidelines for Animal Experiments of Kyushu University and Law 105 Notification 6 of the Japanese Government.

Tumor cells

WEHI3B cells obtained from Dr D. Metcalf (University of Melbourne) and recombinant mouse GM-CSF gene-transduced WEHI3B cell clones, established as previously described[18] were cultured in RPMI 1640 medium (Nacalai Tesque) supplemented with 10% heat-inactivated FBS and 1% penicillin-streptomycin solution (complete medium [CM]).

In vitro cell proliferation assay

WEHI3B and WGM cells were cultured independently in 48-well microplates at 5×10^4 cells/well for 2, 4, and 8 days in CM. On day 2, cells were transferred in 6-well plates and repeated every 2 days thereafter. The number of viable cells was determined by trypan blue dye exclusion assay (Invitrogen).

Tumor models

For the tumorigenicity assay, 5×10^5 cells/100 μL HBSS (Invitrogen) of WEHI3B cells or WGM cells were subcutaneously inoculated into the right flank of WT and BLT1-KO mice, respectively, as first tumor challenge (FTC; n = 6-8 per group). For the second tumor challenge (STC) assay, on day 50 after the subcutaneous inoculation of 5×10^5 cells of WEHI3B cells or WGM cells, 5×10^5 WEHI3B cells were subcutaneously inoculated into the left flank of mice that had completely rejected the challenged WEHI3B cells or WGM cells. Two bisecting diameters of each tumor were measured with calipers, and calculated using the formula $V = 0.4ab^2$, where "a" was the larger diameter and "b" was the smaller diameter of each tumor. Changes in tumor growth were monitored 3 times a week. Mice were killed for ethical reasons when the tumor diameter exceeded 15 mm. The explanatory scheme for all of the following in vivo experiments was illustrated in Figure 1B.

Analyses for tumor-infiltrating leukocytes

Approximately 5×10^6 WGM cells/100 μL were subcutaneously inoculated into the right flank of WT or BLT1-KO mice (n = 3-5 per group). One day after the FTC, the site of tumor inoculation was dissected as described previously.[5] Briefly, tumor tissue was finely minced and digested in RPMI 1640 containing collagenase (Invitrogen) for

20 minutes at 37°C, filtered through a 70-μm strainer, and washed in a fluorescent antibody buffer (FAB) consisting of 0.1% BSA in PBS. Supernatants from tumor tissue were collected, and homogenized cells were blocked with anti-FcR mAb for 15 minutes and followed by staining with either FITC– or PE/Cy7–anti-CD86, PE–anti-CD40, Alexa488– or peridinin-chlorophyll-protein (PerCP)–anti-CCR7, and allophycocyanin (APC)–anti-CD11c mAb either FITC–anti-CD11b, PE–anti-Gr-1, and APC–anti-F4/80, or FITC–anti-DX5, PE–anti-CD107a, and APC– or APC/Cy7–anti-CD3 mAb in FAB for 30 minutes, and subjected to multiparameter flow cytometry, a FACSCalibur or FACSVerse (BD Biosciences). Dead cells were excluded by 7-AAD staining and forward scatter/side scatter FSC/SCC profiles. Analyses of data were performed using FlowJo Version 8.8.6 software (Tree-Star). Concentrations of VEGF, TGF-β, and IL-10 in supernatants from tumor tissues were measured using Quantikine (R&D Systems) or mouse Th1/Th2 ELISA Ready-Set-Go (eBioscience).

MLR

One day after FTC, tumor-draining lymph nodes (TDLNs) and erythrocyte-depleted splenocytes were harvested from WT/WGM or KO/WGM mice as described in "Analyses for tumor-infiltrating leukocytes." DCs as stimulators (S) were purified from splenocytes or TDLNs using CD11c MicroBeads (Miltenyi Biotec). T cells as responders (R) were prepared from isolated splenocytes of C57BL/6 mice using Pan T cell isolation kit II (Miltenyi Biotec), suspended in CM supplemented with 50μM β-mercaptoethanol (Sigma-Aldrich), and cocultured with 30 Gy irradiated DCs at indicated R/T ratios on 96-well U-bottom plate for 4 days. Sixteen hours before the end of culture, 1 μCi [^{3}H]-thymidine (Moravek Biochemicals) was added to each well. Thymidine uptake was quantified in a TopCount NXT (PerkinElmer Life and Analytical Sciences). For CFSE-labeled mixed lymphocyte reaction (MLR) assay, splenic CD11c$^+$ DCs were isolated from WT/WGM or KO/WGM mice using CD11c MicroBeads (Miltenyi Biotec), irradiated with 30 Gy and cocultured with CD3$^+$ T cells as described in this section. After 6 days of coculture, the proliferation rate of CD3$^+$CD4$^+$ or CD3$^+$CD8$^+$ T cells labeled with 2.0μM CFSE (Invivogen) in the coculture was assessed by FACSVerse.

In vivo DC migration assay

Approximately 1×10^7 WGM cells were resuspended in 100 μL diluent C and incubated for 10 minutes with 1×10^{-6} M PKH26 (Sigma-Aldrich). After washing, 5×10^5 PKH26-labeled cells were subcutaneously inoculated into the right flank of WT and BLT1-KO mice. Two days after the FTC, TDLNs were homogenized by mechanical dissociation. Cell suspensions were pretreated with Fc-receptor (FcR) block and stained with FITC–anti-CD86 and APC–anti-CD11c mAb in FAB for 30 minutes. Cells were subjected to FACSCalibur or FACSVerse and analyzed using FlowJo Version 8.8.6 software.

Cytometric bead assay

Cytokine production profile from splenocytes was measured as previously described.[5] Briefly, 1 million splenocytes were harvested from WT or BLT1-KO mice challenged with WEHI3B cells or WGM cells on day 10, depleted of erythrocytes with ammonium chloride, and cocultured with or without 4×10^5 irradiated WEHI3B cells in CM for 20 hours. Production of IL-2, IL-4, IL-5, IFN-γ, and TNF-α in each supernatant was measured using Cytometric Bead Array mouse Th1/Th2 Cytokine kit (BD Biosciences), according to the manufacturer's instructions. Data were analyzed using FCAP Array Version 1.0.1 software (BD Biosciences).

Flow cytometric analysis for intracellular cytokines

On day 46 after the FTC, TDLNs or spleen were harvested from WT/WGM or KO/WGM mice (n = 3-5 per group). Homogenized cells were cultured in CM containing 50μM β-mercaptoethanol, phorbol myristate acetate (10 ng/mL), ionophore (250 mg/mL), and brefeldin A (1 ng/mL) for 4-5 hours. After washing, cells were pretreated with FcR block followed by staining with PerCP-anti–mouse CD4 mAb for 30 minutes. Subsequently, cells were fixed with 2% paraformaldehyde and stained intracellularly with FITC–anti-IFN-γ, PE–anti-IL-4, and APC–anti-IL-17A mAb in permeabilization buffer (eBioscience) for 30 minutes and subjected to FACSCalibur or FACSVerse.

Phenotypic analysis by flow cytometric analysis for diverse immune subpopulations

For mature DCs, TDLNs were harvested from the 4 groups of mice (n = 3 or 4 per group) on days 2 and 4 after the FTC. Obtained cells were blocked with FcR and stained with either FITC–anti-CD86, PE–anti-CD80, and APC–anti-CD11c mAb, or PE–anti-CD40 and APC–anti-CD11c mAb in FAB for 30 minutes. For diverse helper T subsets, TDLNs and splenocytes were harvested from WT/WGM or KO/WGM mice (n = 3-5 per group) on day 46 after the FTC. For memory T subsets, cells were stained with PE–anti-CD44, PerCP–anti-CD4, and APC–anti-CD62L mAb. For regulatory T cells, after staining with FITC–anti-CD3, PE–anti-CD25, and PerCP/Cy5.5–anti-CD4, TDLNs cells were resuspended with 100 μL Fixation/Permeabilization solution (BD Biosciences) and washed with BD Perm/Wash buffer (BD Biosciences) for 20 minutes, followed by the addition of APC–anti–FoxP3 (FJK-16; eBioscience) mAb, and incubated for 30 minutes. For other regulatory T cells, TDLNs and splenocytes were costained with FITC–anti-CD3, PE–anti-GITR, and PerCP–anti-CD4 mAb in FAB for 30 minutes, and subjected to FACSCalibur.

In vivo depletion experiments

GK1.5 and 2.43 hybridoma cells obtained from the Cell Resource Center for Biomedical Research (Institute of Development, Aging and Cancer Tohoku University) were used for the production of anti–mouse CD4 mAb and anti–mouse CD8 mAb, respectively, as previously described.[19] Briefly, these mAbs were purified with centrifugation at 53 000*g* for 20 minutes, and subjected to affinity chromatography using MAb Trap Kit (GE Healthcare). Effective depletion of CD4$^+$ and CD8$^+$ T cells was confirmed by flow cytometric analysis using splenocytes (data not shown). Mice received peritoneal injections of anti–mouse CD4 mAb, anti–mouse CD8 mAb (50 μg per mouse), or PBS for 3 days, and once every 3 days thereafter. For depletion of NK cells, mice received peritoneal injections of rabbit anti-asialo GM1 antiserum (diluted 1:20 in 200 μL PBS; Wako), on 1 day before the STC, and every 7 days thereafter.[20]

Adoptive T-cell transfer experiments

For Th17 adoptive cell transfer (ACT) therapy, Th17 cell preparation was performed as described previously[21] with minor modification. Briefly, splenic CD4$^+$ T cells from WT/WGM or KO/WGM mice on day 46 were magnetic cell sorting (MACS)-sorted using CD4$^+$T cell Isolation kit II(Miltenyi Biotec) and stimulated with plate-bound 1.0 μg/mL anti-CD3 (BD Biosciences) and 1.0 μg/mL anti-CD28 (BD Biosciences) under Th17 conditions with 1.0 ng/mL TGF-β (R&D Systems), 10 ng/mL IL-6 (R&D Systems), 5.0 μg/mL anti–IL-4 (clone 11B11), and 5.0 μg/mL anti–IFN-γ (clone XMG1.2). On day 4 after stimulation with phorbol myristate acetate and ionomycin, Th17 induction rate was confirmed to be ~ 65% among IL-17A–, IL-4–, or IFN-γ–producing T cells, and 1×10^6 cells were then intravenously injected into recipient syngeneic BALB/c mice. On the next day, they received subcutaneous challenge with 2×10^5 WEHI3B cells in the right flank. For CD4$^+$ T-cell ACT therapy, 5×10^5 splenic CD4$^+$CD44^{low} T or CD4$^+$CD44^{hi} T cells harvested from WT/WGM or KO/WGM mice were flow cytometrically (FACSAria, BD Biosciences)-sorted on day 3 after STC and injected intravenously into recipient syngeneic BLAB/c mice. They received subcutaneous challenge with 2×10^5 WEHI3B cells in the right flank.

Statistical analyses

The 2-tailed Student *t* test was used to evaluate *P* values between experimental groups. $P < .05$ was considered statistically significant.

Table 1. Comparison of the number of WGM cell-injected mice that rejected the second tumor challenge with WEHI3B cells between WT and BLT1-KO mice

	Mice that rejected first tumor challenge, no. (%)*	Mice that rejected second tumor challenge, no. (%)†
Female groups‡		
WT/WGM	30/35 (85.7)	9/30 (30.0)§
KO/WGM	16/16 (100)	13/16 (81.3)§
Male groups		
WT/WGM	0/6 (0)	—
KO/WGM	6/6 (100)	5/6 (83.3)§

— indicates not applicable.
*Assessed at day 50 after the first tumor challenge with WEHI3B or WGM cells.
†Assessed at day 50 after the second tumor challenge with WEHI3B cells.
‡Shown are combined pooled data from at least 3 independent experiments with similar results.
§χ^2 test ($P < .05$).

Survival was plotted using Kaplan-Meier curves, and statistical relevance was determined by a log-rank comparison using Prism 5 (GraphPad). All experiments were repeated at least twice.

Results

Absence of LTB4/BLT1 axis in GM-CSF–triggered immunity induces potent antitumor effects against secondary tumor challenge with WEHI3B cells

The GM-CSF production from WEHI3B cells was below detectable levels, whereas that from WGM cells was 136 ng/24 h/10^6 cells (supplemental Figure 1, available on the *Blood* Web site; see the Supplemental Materials link at the top of the online article) enough to induce substantial antitumor effects.[4,8] We compared in vitro proliferative ability between parental WEHI3B and WGM cells. Both cells exhibited an equal proliferation rate in a time-dependent manner (Figure 1A).

As myeloid cells, such as granulocytes, express abundant BLT1 and have direct antitumor effect,[22,23] we speculated that the magnitude of antitumor effect provoked by WGM cells would be attenuated when administered into BLT1-KO mice. To verify our speculation, WEHI3B cells or WGM cells (FTC) were subcutaneously inoculated into the right flank of female WT or BLT1-KO mice. WT mice challenged with WGM cells (WT/WGM mice) rejected tumor growth, whereas WT or BLT1-KO mice challenged with WEHI3B cells (WT/W or KO/W) died of tumor burden. Unexpectedly, BLT1-KO mice challenged with WGM cells (KO/WGM mice) also significantly rejected tumor growth ($P < .05$; Figure 1C). We next compared antitumor responses against secondary tumor challenge with WEHI3B cells long after the FTC rejection. On day 50 after the FTC, parental WEHI3B cells (STC) were subcutaneously inoculated into the opposite (left) flank of WT/WGM and KO/WGM mice that had completely rejected the FTC. Intriguingly, KO/WGM mice significantly again rejected the outgrowth of STC ($P < .01$; Figure 1D) and survived for significantly longer periods compared with WT/WGM mice ($P < .01$; Figure 1E; Table 1). Similar results were observed in experiments using male mice, showing no sexual difference in the STC-rejection mechanism (Table 1).

Previous studies have reported that LTB4 antagonists inhibit cell proliferation of several cancer cells.[24,25] To exclude the possibility that the rejection of STC was attributable to blocking of the LTB4/BLT1 axis-mediated direct antiproliferative effects, we examined BLT1 mRNA levels in WEHI3B and WGM cells by RT-PCR analysis. Both cells expressed undetectable levels of BLT1 mRNA (supplemental Figure 2), showing that the STC rejection was not induced by inhibition of LTB4/BLT1 signaling pathway.

Absence of LTB4/BLT1 axis facilitates activation of tumor-infiltrating innate immune subpopulations with mitigated immune tolerance in GM-CSF-induced antitumor immunity

We hypothesized that the rejection of STC could be induced by memory antitumor immunity. As GM-CSF–producing tumor cell vaccines not only induce the potent antitumor immunity by enhanced maturation of DCs[26] but also simultaneously recruit abundant immune-regulatory myeloid-derived suppressor cells (MDSCs),[27] we investigated the effect of blockade of LTB4/BLT1 signaling on tumor-infiltrating GM-CSF–sensitized diverse subsets of innate immune cells in early phase. The number of MDSCs and macrophages in tumors from KO/WGM mice were significantly decreased compared with those from WT/WGM mice ($P < .05$; Figure 2A-B). In contrast, the cell numbers of tumor-infiltrating NK cells, natural killer-like T cells (NKT), and cytolytic NK cells harvested from KO/WGM mice were significantly increased compared with those from WT/WGM mice (Figure 2C-E). In addition, the defective LTB4/BLT1 axis enhanced maturation of tumor-infiltrating DCs in tumors from KO/WGM mice compared with those from WT/WGM mice, as demonstrated by significantly increased expression of DC maturation markers, such as CD40 and CCR7 ($P < .05$; Figure 2F). Similar results were obtained for $CD86^+CD40^+$DCs, $CD40^+CCR7^+$DCs, $CCR7^+CD86^+$DCs, and $CD86^+CD40^+CCR7^+$DCs isolated from tumors ($P < .05$; Figure 2G-H). We subsequently compared the expression of the immune-regulatory cytokines VEGF, TGF-β, and IL-10 at the tumor injection site that might account for various DC maturation. Concentrations of VEGF, TGF-β, and IL-10 in the supernatants derived from single-cell suspensions of excised tumors from KO/WGM mice were significantly lower than those of WT/WGM mice ($P < .05$; Figure 2I). Lastly, to examine the effect of the defective LTB4/BLT1 axis on GM-CSF–primed DCs for T-cell activation, we performed MLR assay using allogeneic T cells from C57BL/6 mice and splenic- or TDLN-derived $CD11c^+$ DCs. The results showed that both splenic- (Figure 2J left panel) and TDLN- (Figure 2J right panel) derived DCs harvested from KO/WGM mice stimulated $CD3^+$ T cells more efficiently than those from WT/WGM mice. When we compared the stimulation capacity of DCs harvested from KO/WGM mice for $CD4^+$ and $CD8^+$ T cells, we observed a superior proliferation of $CD4^+$ T cells but not $CD8^+$ T cells (Figure 2K).

Absence of LTB4/BLT1 axis augments maturation and migration capacity of phagocytosed TAAs-DCs in GM-CSF-induced antitumor immunity

We next evaluated the impact of the defective LTB4/BLT1 axis on maturation of DCs in TDLNs on day 2 or 4 after FTC. As shown in Figure 3A-C and supplemental Figure 3, the mean fluorescence intensity of each CD40, CD80, and CD86 expression on DCs in TDLNs from KO/WGM mice was significantly more increased than that from WT/WGM mice ($P < .05$). To determine the influence of the defective LTB4/BLT1 axis on the migration

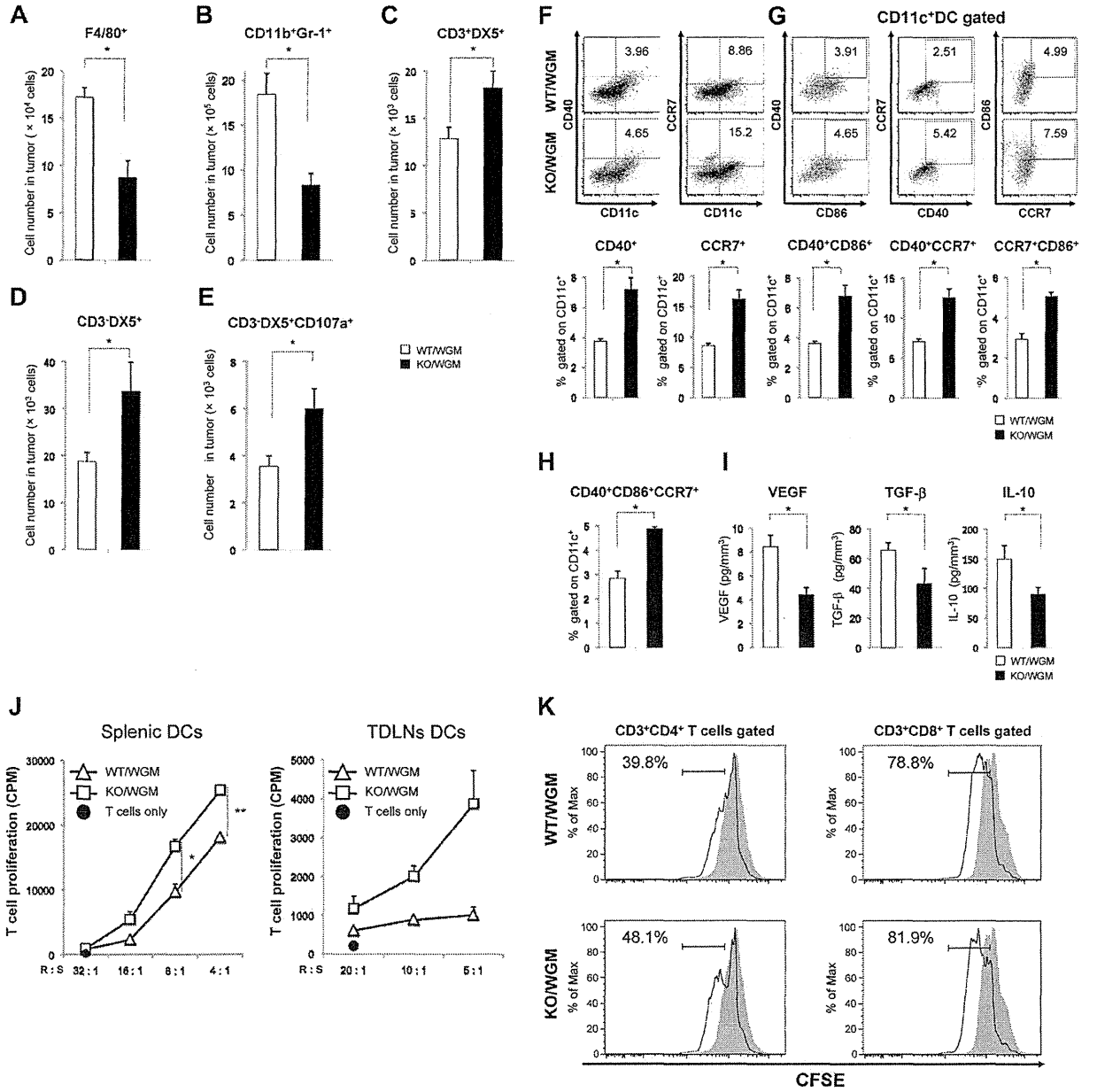

Figure 2. Absence of LTB4/BLT1 signaling promotes activation of various innate immune subpopulations in tumor tissues, accompanied with attenuated immune tolerance in KO/WGM mice. (A-E) One day after the FTC with WGM cells, tumors were excised from WT/WGM or KO/WGM mice, minced finely, and treated with collagenase for tissue dissociation. For assessment of innate immunity subpopulations, tumor infiltrating cells were subsequently analyzed by flow cytometry as described in "Analyses for tumor-infiltrating leukocytes." The numbers of viable cells are shown. (F-H) For detection of mature DCs, cells were stained with anti-CD11c, anti-CD40, anti-CD86, and anti-CCR7 mAb and subjected to flow cytometric analysis. Results shown are representative 2-dimensional dot plots (top panel, F-G) and bar graphs depicting the rates of indicated tumor infiltrating mature DCs (bottom panel, F-G). Numbers in 2-dimensional dot plots reflect the frequencies of (F) $CD40^+$ or $CCR7^+CD11c^+$cells, (G) $CD40^+CD86^+$, $CD40^+CCR7^+$, or $CCR7^+CD86^+CD11c^+$cells, and (H) $CD40^+CD86^+CCR7^+CD11c^+$ cells relative to the total $CD11c^+$ cells. (I) The concentrations of VEGF ($n = 5$ or 6), TGF-β ($n = 3$), and IL-10 ($n = 9$ or 10) in supernatants derived from smashed tumor tissue of WT/WGM or KO/WGM mice were measured by ELISA assay. (J) MLR assay evaluated by [^{3}H]thymidine incorporation. Various numbers of MACS-sorted splenic (left panel)- or TDLNs (right panel)-derived $CD11c^+$ DCs from WT/WGM or KO/WGM mice in early phase were 30 Gy irradiated as stimulator cells and incubated with 2×10^5 MACS-sorted splenic $CD3^+$ T cells (responder) harvested from splenic C57BL/6 mice at responder to stimulator (R:S) ratios as indicated for 4 days in triplicate. [^{3}H]Thymidine was added 16 hours before the cells were harvested, and thymidine incorporation was assessed using TopCount NXT microplate scintillation counter. Cultures in the absence of DCs (T cells only) were used as a negative control. (K) CFSE-labeled MLR assay. A total of 100 000 MACS-sorted splenic $CD11c^+$ DCs were harvested from WT/WGM or KO/WGM mice, irradiated with 30 Gy, and cocultured with $CD3^+$ T cells at an R:S ratio of 2:1. After 6 days of coculture, the proliferation rate of $CD3^+CD4^+$ T cells (left panel) or $CD3^+CD8^+$ T cells (right panel) labeled with 2.0μM CFSE in the coculture was assessed by flow cytometric analysis. The histograms are gated on $CD3^+CD4^+$ or $CD3^+CD8^+$ T cells. Cultures in the absence of DCs (T cells only) were used as a negative control. Bar graphs represent mean ± SEM. *Significant difference ($P < .05$). **Significant difference ($P < .01$). Representative data from 3 independent experiments or combined data from 2 independent experiments (D-E) with similar results are shown.

capacity of mature DCs that had engulfed TAAs into TDLNs, we compared a proportion of $CD86^+PKH26^+$ DCs in TDLNs between WT/WGM and KO/WGM mice on day 2 after the FTC. The frequency of $CD86^+PKH26^+$ DCs in TDLNs harvested from KO/WGM mice was > 5-fold higher than that from WT/WGM mice (Figure 3D).

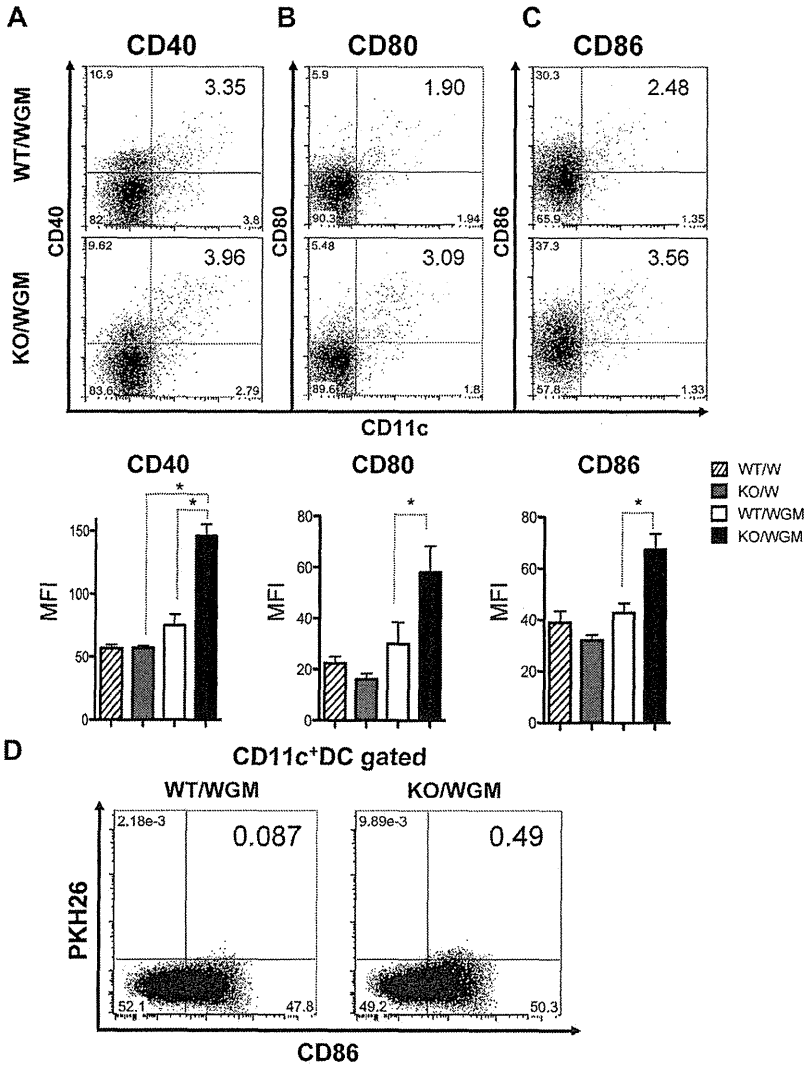

Figure 3. Absence of LTB4/BLT1 axis enhances maturation of DCs and recruitment of TAA-phagocytosed DCs into TDLNs in KO/WGM mice in early phase. Two left axillary TDLNs were harvested from WT/W, KO/W, WT/WGM, or KO/WGM mice on day 2 (CD80 and CD86) or day 4 (CD40) after the tumor challenge (n = 3-5 per group). Data are representative dot plots (top panel) and the averages of mean fluorescence intensity (bottom panel) for $CD11c^+$ cells expressing the following markers of (A) CD40, (B) CD80, or (C) CD86 in TDLNs harvested from 4 indicated experimental groups. Bar graphs represent mean ± SEM. *Significant difference ($P < .05$). (D) Migration of DCs that had phagocytosed TAAs to TDLNs in WT/WGM or KO/WGM mice on day 2 after the subcutaneous inoculation with PKH26-labeled WGM cells. Numbers in 2-dimensional dot plots reflect the positive ratio of $PKH26^+CD86^+$ cells relative to total $CD11c^+$ cells. Representative data from at least 3 independent experiments with similar results are shown.

Absence of LTB4/BLT1 axis in GM-CSF–induced antitumor immunity systemically enhances TAAs-specific Th1 and Th2 responses in intermediate phase

To characterize the immune-modulatory effects of the defective LTB4/BLT1 axis on GM-CSF–triggered adaptive immunity, the expression levels of inflammatory cytokines, IL-2, IFN-γ, TNF-α (Th1 cytokines), and IL-4 and IL-5 (Th2 cytokines) secreted from splenocytes harvested from KO/WGM mice were compared with those from WT/WGM mice. On the coculture with irradiated WEHI3B cells, the expression levels of IL-2, IFN-γ, TNF-α, IL-4, and IL-5 from KO/WGM mice, on day 10 after FTC, were increased compared with those from WT/WGM mice. Only levels of IL-4 were significantly altered. All other cytokines tested did not show significant differences between the 2 groups but exhibited the same tendency in 3 independent experiments (Figure 4A-E).

Absence of LTB4/BLT1 axis in GM-CSF-induced antitumor immunity increases diverse memory $CD4^+$ T subsets skewing Th balance toward Th2 and Th17 predominance with antitumor phenotype

We speculated that the defective LTB4/BLT1 axis could have a positive impact on phenotypic profile of different memory $CD4^+$ or $CD8^+$ T subset, which might account for the marked rejection of STC. Thus, we compared the rates of central memory T subset (T_{CM}) and effector memory T subset (T_{EM}) in TDLNs between WT/WGM and KO/WGM mice on day 46 in late phase. Surface marker of CD44 was used as memory phenotype. TDLNs harvested from KO/WGM mice contained significantly higher proportions of the $CD4^+CD44^+CD62L^+$ (T_{CM}) and $CD4^+CD44^+CD62L^-$ (T_{EM}) subsets relative to the total $CD4^+$ T-cell population compared with those from WT/WGM mice ($P < .05$; Figure 5A), suggesting that the defective LTB4/BLT1 axis could serve to generate long-surviving TAA-specific memory $CD4^+$ T cells. Subsequently, the proportion of Th1, Th2, and Th17 subsets in TDLNs and spleen in the late phase was evaluated between the 2 groups. The results showed that the frequency of Th2 and Th17 subset in TDLNs from KO/WGM mice increased by 32% and 47%, respectively, compared with that from WT/WGM mice (data not shown), indicating that the defective LTB4/BLT1 axis in GM-CSF–triggered immunity could cause a shift of the Th balance toward Th2 and Th17 predominance. Because IL-4 production fromTh2 cells is reported to be essential for maximal systemic antitumor immunity induced by GM-CSF–based tumor immunization,[4,28] we analyzed the total number of IL-4–producing $CD4^+$ T cells from TDLNs between the 2 groups. The total number of IL-4–producing

Th2 cells in TDLNs from KO/WGM mice was significantly higher than in WT/WGM mice ($P < .05$), suggesting that the defective LTB4/BLT1 axis facilitates effective induction of antitumor Th2 responses driven by GM-CSF (Figure 5B). To determine whether the Th17 subset has an in vivo antitumor activity, we treated recipient BALB/c mice with adoptive cell transfer of splenic Th17-skewed cells derived from WT/WGM or KO/WGM mice and subcutaneously challenged them with parental WEHI3B cells. Only the transfer of KO/WGM mice-derived Th17 cells significantly suppressed the WEHI3B tumor development compared with untreated and WT/WGM mice ($P < .05$; Figure 5C).

Furthermore, we evaluated the effect of the defective LTB4/BLT1 axis on regulatory T-cell subpopulations. The each percentage of $CD4^+CD25^+FoxP3^+$ regulatory T cells or $CD3^+CD4^+GITR^+$ cells between WT/WGM and KO/WGM mice was comparatively assessed, as GITR expression is constitutively up-regulated in regulatory T cells but not on resting $CD3^+CD4^+$ T lymphocytes.[29,30] The percentages of $CD4^+CD25^+Foxp3^+$ regulatory T cells in TDLNs and $CD3^+CD4^+GITR^+$ T cells in TDLNs and spleen from KO/WGM mice were more decreased than those from WT/WGM mice (Figure 5D-E).

Marked rejection of STC in KO/WGM mice is mainly attributed to $CD4^+$ T cells where memory Th subset possesses an antitumor phenotype

In vivo depletion of $CD4^+$ T, $CD8^+$ T, and NK cells was performed to determine which subsets are essential for the rejection of STC

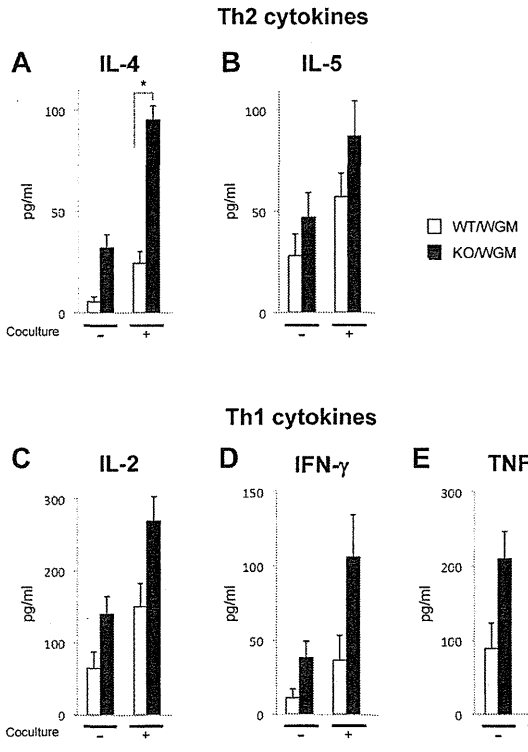

Figure 4. Absence of LTB4/BLT1 axis promotes systemic activation of TAA-specific Th1 and Th2 subsets in KO/WGM mice in intermediate phase. In vitro Th1/Th2 cytokine production profiles of splenocytes harvested from WT/W, KO/W, WT/WGM, or KO/WGM mice on day 10 after the FTC. Approximately 1×10^6 splenocytes harvested were cultured with or without 4×10^5 irradiated WEHI3B cells for 20 hours. The concentrations of mouse (A) IL-4, (B) IL-5, (C) IL-2, (D) IFN-γ, and (E) TNF-α in the culture supernatants (n = 3) were measured by cytometric bead array assay. Bar graphs represent mean ± SEM. *Significant differences ($P < .05$). Representative data from 3 independent experiments with similar results are shown.

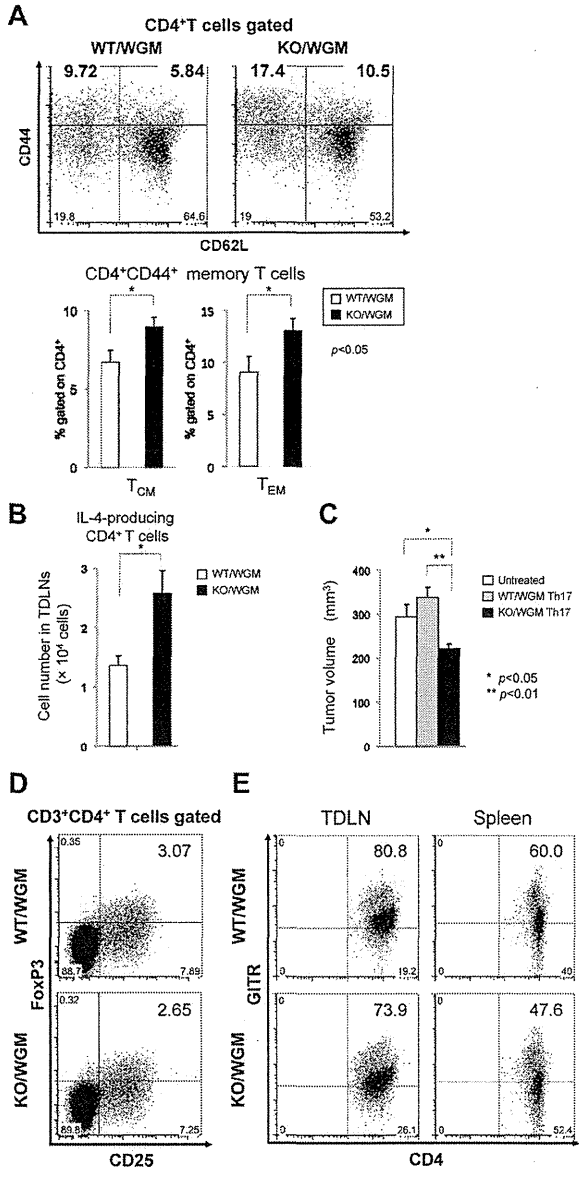

Figure 5. Absence of LTB4/BLT1 axis facilitates induction of diverse memory $CD4^+$ T subsets and polarized Th2/Th17 cells with antitumor phenotype in KO/WGM mice in late phase. TDLNs cells harvested from WT/WGM or WT/WGM mice (n = 3-5/group) on day 46 after the FTC were subjected to polychromatic flow cytometric analyses. (A) Dot plot profiles (top panels) and graphs (bottom panels) represent the percentages of $CD4^+CD44^+CD62L^+$ T_{CM} or $CD4^+CD44^+CD62L^-$ T_{EM} subset relative to the total $CD4^+$ T-cell population. Numbers in boldface in dot plot profiles show the representative percentages of T_{CM} and T_{EM} in WT/WGM and KO/WGM and are reflected to the graphs. (B) Bar graphs represent the total number of IL-4-producing T cells in TDLNs derived from WT/WGM and KO/WGM mice (n = 3 or 4). Combined data from 2 independent experiments are shown. (C) Th17 adoptive T-cell transfer (ACT) assay. Splenic $CD4^+$ T cells from WT/WGM or KO/WGM mice on day 46 were MACS-sorted and stimulated with plate-bound anti-CD3 mAb and soluble anti-CD28 mAb under Th17 condition. After 4 days of incubation, 1 million cells were intravenously transferred into recipient syngeneic BALB/c mice. On the next day, they received subcutaneous challenge with WEHI3B cells in the right flank. Bar graph represents the tumor volume (mm^3) of untreated, mice treated with WT/WGM mice- or KO/WGM mice-derived Th17 ACT, assessed on day 10 after the Th17 ACT therapy. (D-E) Phenotypic profile of immune-regulatory T cells in late phase. Shown are representative dot plots depicting the percentages of (D) $CD3^+CD4^+CD25^+FoxP3^+$ cells in TDLNs harvested from WT/WGM or KO/WGM mice, and of (E) $CD3^+CD4^+GITR^+$ T cells in TDLNs and spleen from WT/WGM or KO/WGM mice. Bar graphs represent the mean ± SEM. Significant differences: $^*P < .05$, $^{**}P < .01$. Representative data from 3 independent experiments with similar results or combined data (A-C) from 2 independent experiments are shown.

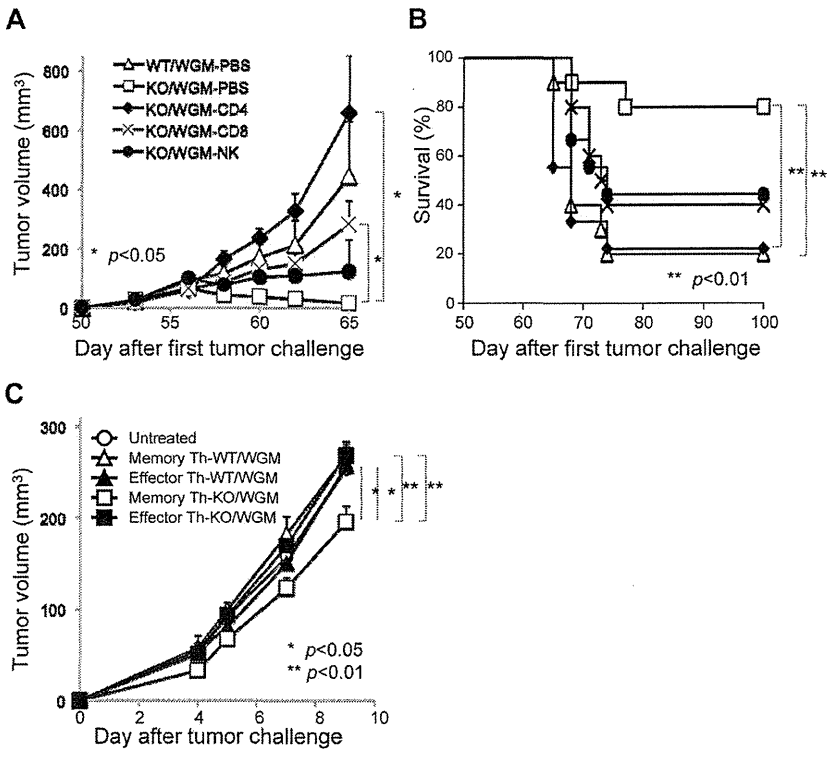

Figure 6. CD4+ T cells mainly mediate the remarkable rejection of second tumor challenge with WEHI3B cells where memory CD44hiCD4+ T subset has an antitumor phenotype on adoptive cell transfer. All mice that had completely rejected the FTC with WGM cells were then subcutaneously inoculated with the STC on day 50 after the FTC, as described in Figure 1 (n = 4-6). For depletion of CD4+ and CD8+ T cells, mice received repeated intraperitoneal injections of anti–mouse-CD4 mAb or anti–mouse-CD8 mAb on days 3, 4, and 5 before the day of the STC and once every 3 days thereafter up to 13 times. For depletion of NK cells, mice received repeated intraperitoneal injections of rabbit anti-asialo GM1 antiserum 1 day before and 7 and 14 days after the STC. (A) Tumor volume was monitored and (B) a survival curve of the mice groups was examined. (C) For CD4+ T-cell ACT therapy, 5×10^5 CD4+CD44low or CD4+CD44hi T cells harvested from spleen of WT/WGM or KO/WGM mice were flow cytometrically sorted on day 3 after the STC and intravenously injected into recipient syngeneic BLAB/c mice (n = 4-6). On the next day, they received subcutaneous challenge with 2×10^5 parental WEHI3B cells in the right flank. Bar graphs represent mean ± SEM. Significant differences: *$P < .05$, **$P < .01$. Representative or combined data from 2 independent experiments with similar results are shown.

seen in KO/WGM mice. Each depletion of CD4+ T, CD8+ T, or NK cells in KO/WGM mice significantly abrogated the antitumor effects compared with PBS-treated KO/WGM mice ($P < .05$). Importantly, KO/WGM mice depleted of CD4+ T cells elicited rather accelerated tumor outgrowth (Figure 6A) and a significantly shorter survival (Figure 6B), with a significant decrease in number of mice that rejected the STC (Table 2), compared with WT/WGM mice, demonstrating that the long-lasting antitumor immunity seen in KO/WGM mice was largely dependent on CD4+ T cells.

To determine whether the persistent antitumor memory observed in KO/WGM mice was memory CD4+ T subset-dependent, we comparatively investigated therapeutic effects by adoptive T-cell transfer (ACT) between CD4+CD44low T cells (effector Th) and CD4+CD44hi T (memory Th) cells, both of which were sorted from spleens of WT/WGM or KO/WGM mice on day 3 after the STC. We treated mice with intravenous ACT therapy and, on the next day, challenged them with WEHI3B cells in the right flank. Either with or without ACT using KO/WGM mice-derived effector Th subset, WEHI3B tumors continued to grow, whereas ACT using KO/WGM mice-derived splenic memory Th subset significantly inhibited the WEHI3B tumor formation (Figure 6C). On the other hand, all ACT therapies using cells from WT/WGM mice manifested no antitumor activity. These results strongly indicated that memory Th subset has an important role in GM-CSF–induced antitumor memory immunity when the LTB4/BLT1 signaling is not present or dysfunctional.

Table 2. Effect of in vivo depletion of each immune subpopulation on the long-lasting rejection of the second tumor challenge

Group	Mice that rejected second tumor challenge, no. (%)*
WT/WGM-PBS	1/10 (10.0)†
KO/WGM-PBS	9/11 (81.8)
KO/WGM-CD4	1/10 (10.0)†
KO/WGM-CD8	3/11 (27.3)†
KO/WGM-NK	2/10 (20.0)†

Shown are combined pooled data from 2 independent experiments with similar results.

*Assessed at day 15 after the second tumor challenge with WEHI3B cells.

†χ^2 test ($P < .05$).

Discussion

Memory T cells respond promptly to delivered antigens and are critical in the induction of sustained antitumor immunity. They require less costimulation to be activated and release a broader spectrum of cytokines compared with naive T cells.[31] One of the major challenges for therapeutic improvement of cancer vaccines is to optimize persistent memory antitumor responses.

Numerous studies reported that leukotrienes are involved in carcinogenesis and tumor development.[24,25,32,33] However, the role of leukotriene-based signaling in tumor immunology, including memory immunity, has never been elucidated. In the current study, we are the first group to find that the defective LTB4/BLT1 signaling induces long-term antitumor memory responses after immunization with WGM cells, demonstrating that the LTB4/BLT1 axis is an adversary for maintaining GM-CSF–triggered antitumor memory responses as summarized in a schematic overview (Figure 7). Namely, blockade of the LTB4/BLT1 signaling elicited numerous positive effects on development of GM-CSF–triggered persistent antitumor memory immunity as follows:

1. The defective LTB4/BLT1 axis diminished the recruitment of immune-regulatory MDSCs into tumors in early phase (Figure 2B), probably because of abundant BLT1 expression in diverse myeloid cells, including MDSCs.[34]

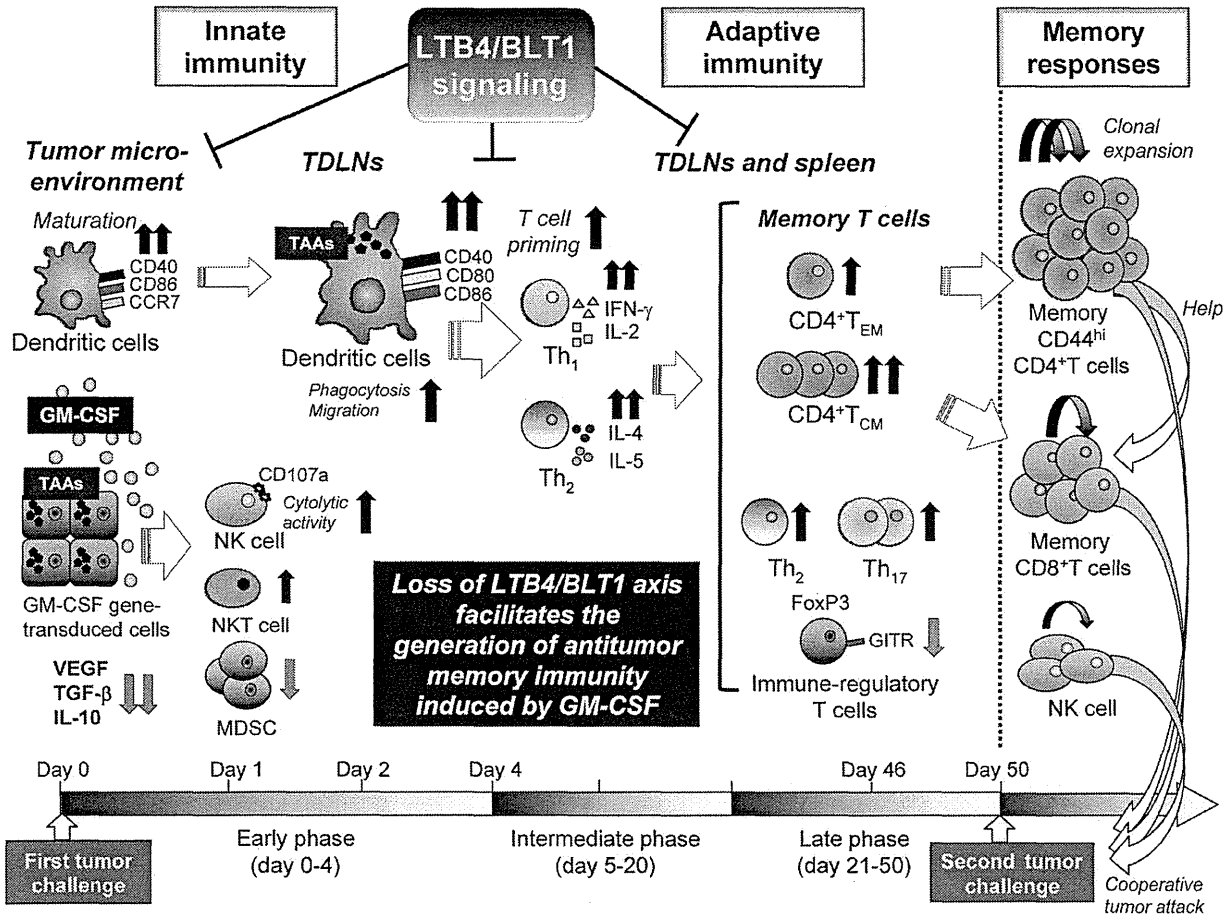

Figure 7. Schematic overview of the experimental results. This schematic overview illustrates the effects of the defective LTB4/BLT1 axis on the process of generation of antitumor memory immunity provoked by GM-CSF–transduced tumor cells in mice, and the molecular or cellular components that compose the immune system and are putatively relevant to this phenomenon.

2. The absence of LTB4/BLT1 axis increased recruitment of CD107a, a surrogate for lytic degranulation,[35] expressing cytolytic NK cells into tumors (Figure 2E), indicating its negative effects for tumoricidal ability activated by GM-CSF.
3. The defective LTB4/BLT1 signaling caused a synergistic effect on maturation, homing capacity of TAA-phagocytosed DCs into TDLNs (Figures 2F-H and 3A-D), and further enhanced the capacity of GM-CSF–sensitized DCs to stimulate $CD4^+$ T cells, but not $CD8^+$ T cells (Figure 2J-K), indicating its effective priming of helper T cell-predominant adaptive immunity. These positive effects on DCs were the result of the decreased expression of various immune-regulatory cytokines in tumor microenvironments (Figure 2I). On the contrary, others reported that LTB4 stimulation enhances DC migration and adaptive immune responses.[13] This discrepancy may stem from our use of GM-CSF gene-transduced tumor cells, although the detailed molecular crosstalk between LTB4/BLT1 and GM-CSF signaling remains unknown.
4. The absence of LTB4/BLT1 axis augmented the production of Th1 cytokine and Th2 cytokine from TAA-stimulated splenocytes harvested from GM-CSF–sensitized mice in intermediate phase (Figure 4). Conversely, Toda et al showed that functional BLT1 expression on DCs is important to initiate Th1-type immune response, indicating that GM-CSF–based immunization may bring about the conflicting outcome.[36]
5. The absence of LTB4/BLT1 axis increased the proportions of $CD4^+$ T_{CM} and $CD4^+$ T_{EM} subset in TDLNs in late phase before the STC (Figure 5A). As memory T cells possess the capacity to mount immediate recall responses to antigen challenge[37] and that T_{CM} subset has superior antitumor abilities compared with T_{EM} subset,[38] we hypothesized that the former subset might rapidly migrate to the injection site of STC to confer antitumor effects. Indeed, we succeeded to demonstrate that the KO/WGM mice-derived memory Th subset had significantly stronger antitumor efficacy than the effector Th subset from the results of ACT therapy (Figure 6C).
6. We showed that the defective LTB4/BLT1 signaling in GM-CSF-triggered antitumor immunity skewed Th2 predominance in late phase (Figure 5B) and that ACT of splenic Th17 cells harvested from KO/WGM mice elicited stronger antitumor effects against WEHI3B challenge than those from WT/WGM mice (Figure 5C). Our results are compatible with the previous reports showing that memory Th2 cells had a potent antitumor immunity through IL-4–activated NK cells[39] and that the Th17 subset was decisive for yielding immunologic responses together with effector cytotoxic T lymphocytes.[40] These findings indicate that the

absence of LTB4/BLT1 signaling facilitates Th2 and Th17 polarization with antitumor phenotype, although the significance of Th2 and Th17 cells in tumor immunology is still controversial.[41,42] As frequency of multifunctional $CD4^+$ T cells simultaneously producing IFN-γ, IL-2, and TNF-α is recognized as a sensitive immune correlate for the optimized effector function against antigens,[43] we assessed the influence of the defective LTB4/BLT1 signaling on phenotypic profiles of $CD4^+$ T-cell multifunctionality. There was, however, no significant difference in frequency of each single-, or double-, or triple-cytokine producing $CD4^+$ T subset between WT/WGM and KO/WGM mice (supplemental Figure 4).

7. The absence of LTB4/BLT1 in GM-CSF–induced immunity systemically decreased production levels of the immune-regulatory cytokines in the tumor microenvironment (Figure 2I) and the infiltrated immune-regulatory $CD4^+$ T subsets in lymphoid tissue (Figure 5D-E), probably converting the immunosuppressive milieu to one that helps both generation and maintenance of memory T cells. Although other researchers showed that LTB4 plus IL-2 could generate $CD8^+$ suppressor thymocytes involved in tolerance to self-antigens,[44] there have never been relevant data delineating relationship between arachidonic-acid–derived lipid mediator, such as pro-inflammatory leukotrienes and regulatory T cell-mediated immune tolerance. Thereby, our findings could offer a hint to attenuate tumor-driven immune tolerance via the inhibition of the LTB4/ BLT1 signaling.
8. Finally, our results from in vivo depletion assays unraveled that $CD4^+$ T cells in KO/WGM mice played a predominant role in providing persistent antitumor immunity, in coordination with NK cells and $CD8^+$ T cells (Figure 6A-B), which are compatible with the previous findings that $CD4^+$ T cells are essential in the control of tumor growth through the cooperation with macrophages and cytotoxic T lymphocytes.[4,45,46] When we consider to further clarify the molecular crosstalk between LTB4 and GM-CSF signaling pathways, it will be of importance to focus on our findings that the absence of the LTB4/BLT1 axis had positive impact mainly on $CD4^+$ helper T cell-mediated adaptive immunity as evidenced by MLR assay and ACT experiments, as well as innate immunity. This novel insight that potent memory $CD4^+$ T cells in GM-CSF–triggered immunity can be retained in devoid of LTB4/BLT1signaling allows us to expect that blocking LTB4/BLT1signaling using corresponding antagonists or inhibitors may be a promising strategy to improve the therapeutic effects of GM-CSF–based tumor vaccines in clinical settings by shaping a favorable immunologic memory.

With regard to another receptor BLT2 for LTB4, it requires very high concentrations of LTB4 for its activation[47] and has been well accepted to be a receptor for 12-HHT.[48] Accordingly, it is now thought that BLT2 does not mediate any functions of LTB4 in the absence of BLT1 in vivo. We therefore disregarded the impact of BLT2 on the results of our experiments.

Intriguingly, in terms of sexual difference, the mechanism in which a superior antitumor immunity induced by WGM cells was manifested in WT female mice compared with WT male (Table 1) could possibly be explained by the following WT regulatory T cells from female mice expressing significantly lower B7-H1, a coinhibitory signaling molecule that can suppress antitumor immunity[49] and possess a more efficient phagocytic ability by resident macrophages,[50] compared with those from male mice.

In conclusion, we demonstrated that, even long after the tumor rejection, the defective LTB4/BLT1 axis facilitates effective generation of long-lasting memory $CD4^+$ T cell-dependent antitumor immunity through its positive impacts on innate and adaptive immunologic responses induced by GM-CSF.

Acknowledgments

The authors thank Dr Kazuko Saeki and Dr Toshiaki Okuno (Kyushu University) for their technical supports.

This work was supported in part by the Japan Society for the Promotion of Science (Grant-in-Aid for Young Scientists 23790446) and the Ministry of Education, Culture, Sports, Science and Technology, Japan (Grant-in-Aid for Scientific Research on Priority Areas "Cancer" 17016053).

Authorship

Contribution: Y.Y., H.I., and K. Tani designed the study and wrote manuscript; Y.Y., H.I., Y.M., C.S., and H.N. executed the experiments; Y.Y. analyzed all data; Y.Y., H.I., T.Y., and K. Tani interpreted the results of experiments; Y.Y., H.N., A.W., and F.S. contributed in the backcross and preparation of mice; and all authors discussed the results and helped conduct experiments.

Conflict-of-interest disclosure: The authors declare no competing financial interests.

Correspondence: Kenzaburo Tani, Department of Molecular Genetics, Medical Institute of Bioregulation, Kyushu University, 3-1-1, Maidashi, Higashi-ku, Fukuoka, Japan 812-8582; e-mail: taniken@bioreg.kyushu-u.ac.jp.

References

1. Jinushi M, Tahara H. Cytokine gene-mediated immunotherapy: current status and future perspectives. *Cancer Sci.* 2009;100(8):1389-1396.
2. Tani K, Azuma M, Nakazaki Y, et al. Phase I study of autologous tumor vaccines transduced with the GM-CSF gene in four patients with stage IV renal cell cancer in Japan: clinical and immunological findings. *Mol Ther.* 2004;10(4):799-816.
3. Dranoff G. GM-CSF-based cancer vaccines. *Immunol Rev.* 2002;188:147-154.
4. Dranoff G, Jaffee E, Lazenby A, et al. Vaccination with irradiated tumor cells engineered to secrete murine granulocyte-macrophage colony-stimulating factor stimulates potent, specific, and long-lasting anti-tumor immunity. *Proc Natl Acad Sci U S A.* 1993;90(8):3539-3543.
5. Inoue H, Iga M, Nabeta H, et al. Non-transmissible Sendai virus encoding granulocyte macrophage colony-stimulating factor is a novel and potent vector system for producing autologous tumor vaccines. *Cancer Sci.* 2008;99(11):2315-2326.
6. Salgia R, Lynch T, Skarin A, et al. Vaccination with irradiated autologous tumor cells engineered to secrete granulocyte-macrophage colony-stimulating factor augments antitumor immunity in some patients with metastatic non-small-cell lung carcinoma. *J Clin Oncol.* 2003;21(4):624-630.
7. Ho VT, Vanneman M, Kim H, et al. Biologic activity of irradiated, autologous, GM-CSF-secreting leukemia cell vaccines early after allogeneic stem cell transplantation. *Proc Natl Acad Sci U S A.* 2009;106(37):15825-15830.
8. Nakazaki Y, Hase H, Inoue H, et al. Serial analysis of gene expression in progressing and regressing mouse tumors implicates the involvement of RANTES and TARC in antitumor immune responses. *Mol Ther.* 2006;14(4):599-606.
9. Simmons AD, Li B, Gonzalez-Edick M, et al. GM-CSF-secreting cancer immunotherapies: preclinical analysis of the mechanism of action. *Cancer Immunol Immunother.* 2007;56(10):1653-1665.
10. Eager R, Nemunaitis J. GM-CSF gene-transduced tumor vaccines. *Mol Ther.* 2005;12(1):18-27.

11. Lewis RA, Austen KF, Soberman RJ. Leukotrienes and other products of the 5-lipoxygenase pathway: biochemistry and relation to pathobiology in human diseases. *N Engl J Med.* 1990; 323(10):645-655.
12. Naccache PH, Sha'afi RI. Arachidonic acid, leukotriene B4, and neutrophil activation. *Ann N Y Acad Sci.* 1983;414:125-139.
13. Del Prete A, Shao WH, Mitola S, Santoro G, Sozzani S, Haribabu B. Regulation of dendritic cell migration and adaptive immune response by leukotriene B4 receptors: a role for LTB4 in up-regulation of CCR7 expression and function. *Blood.* 2007;109(2):626-631.
14. Yokomizo T, Izumi T, Chang K, Takuwa Y, Shimizu T. A G-protein-coupled receptor for leukotriene B4 that mediates chemotaxis. *Nature.* 1997;387(6633):620-624.
15. Griffin JD, Cannistra SA, Sullivan R, Demetri GD, Ernst TJ, Kanakura Y. The biology of GM-CSF: regulation of production and interaction with its receptor. *Int J Cell Cloning.* 1990;Suppl 1:35-44.
16. Miller G, Pillarisetty VG, Shah AB, Lahrs S, Xing Z, DeMatteo RP. Endogenous granulocyte-macrophage colony-stimulating factor overexpression in vivo results in the long-term recruitment of a distinct dendritic cell population with enhanced immunostimulatory function. *J Immunol.* 2002;169(6):2875-2885.
17. Terawaki K, Yokomizo T, Nagase T, et al. Absence of leukotriene B4 receptor 1 confers resistance to airway hyperresponsiveness and Th2-type immune responses. *J Immunol.* 2005; 175(7):4217-4225.
18. Nakazaki Y, Tani K, Lin ZT, et al. Vaccine effect of granulocyte-macrophage colony-stimulating factor or CD80 gene-transduced murine hematopoietic tumor cells and their cooperative enhancement of antitumor immunity. *Gene Ther.* 1998; 5(10):1355-1362.
19. Kruisbeek AM. In vivo depletion of CD4- and CD8-specific T cells. *Curr Protoc Immunol.* 1991; Chapter 4:Unit 4 1.
20. Inoue H, Iga M, Xin M, et al. TARC and RANTES enhance antitumor immunity induced by the GM-CSF-transduced tumor vaccine in a mouse tumor model. *Cancer Immunol Immunother.* 2008;57(9): 1399-1411.
21. Nurieva R, Yang XO, Chung Y, Dong C. Cutting edge: in vitro generated Th17 cells maintain their cytokine expression program in normal but not lymphopenic hosts. *J Immunol.* 2009;182(5): 2565-2568.
22. Koga Y, Matsuzaki A, Suminoe A, Hattori H, Hara T. Neutrophil-derived TNF-related apoptosis-inducing ligand (TRAIL): a novel mechanism of antitumor effect by neutrophils. *Cancer Res.* 2004;64(3):1037-1043.
23. Di Carlo E, Forni G, Lollini P, Colombo MP, Modesti A, Musiani P. The intriguing role of polymorphonuclear neutrophils in antitumor reactions. *Blood.* 2001;97(2):339-345.
24. Tong WG, Ding XZ, Hennig R, et al. Leukotriene B4 receptor antagonist LY293111 inhibits proliferation and induces apoptosis in human pancreatic cancer cells. *Clin Cancer Res.* 2002;8(10): 3232-3242.
25. Ihara A, Wada K, Yoneda M, Fujisawa N, Takahashi H, Nakajima A. Blockade of leukotriene B4 signaling pathway induces apoptosis and suppresses cell proliferation in colon cancer. *J Pharmacol Sci.* 2007;103(1):24-32.
26. Mach N, Gillessen S, Wilson SB, Sheehan C, Mihm M, Dranoff G. Differences in dendritic cells stimulated in vivo by tumors engineered to secrete granulocyte-macrophage colony-stimulating factor or Flt3-ligand. *Cancer Res.* 2000;60(12): 3239-3246.
27. Serafini P, Carbley R, Noonan KA, Tan G, Bronte V, Borrello I. High-dose granulocyte-macrophage colony-stimulating factor-producing vaccines impair the immune response through the recruitment of myeloid suppressor cells. *Cancer Res.* 2004;64(17): 6337-6343.
28. Hung K, Hayashi R, Lafond-Walker A, Lowenstein C, Pardoll D, Levitsky H. The central role of CD4(+) T cells in the antitumor immune response. *J Exp Med.* 1998;188(12):2357-2368.
29. Shimizu J, Yamazaki S, Takahashi T, Ishida Y, Sakaguchi S. Stimulation of CD25(+)CD4(+) regulatory T cells through GITR breaks immunological self-tolerance. *Nat Immunol.* 2002;3(2): 135-142.
30. Nocentini G, Riccardi C. GITR: a multifaceted regulator of immunity belonging to the tumor necrosis factor receptor superfamily. *Eur J Immunol.* 2005;35(4):1016-1022.
31. Veiga-Fernandes H, Walter U, Bourgeois C, McLean A, Rocha B. Response of naive and memory CD8+ T cells to antigen stimulation in vivo. *Nat Immunol.* 2000;1(1):47-53.
32. Hoque A, Lippman SM, Wu TT, et al. Increased 5-lipoxygenase expression and induction of apoptosis by its inhibitors in esophageal cancer: a potential target for prevention. *Carcinogenesis.* 2005;26(4):785-791.
33. Avis IM, Jett M, Boyle T, et al. Growth control of lung cancer by interruption of 5-lipoxygenase-mediated growth factor signaling. *J Clin Invest.* 1996;97(3):806-813.
34. Yokomizo T. Leukotriene B4 receptors: novel roles in immunological regulations. *Adv Enzyme Regul.* 2011;51(1):59-64.
35. Alter G, Malenfant JM, Altfeld M. CD107a as a functional marker for the identification of natural killer cell activity. *J Immunol Methods.* 2004; 294(1):15-22.
36. Toda A, Terawaki K, Yamazaki S, Saeki K, Shimizu T, Yokomizo T. Attenuated Th1 induction by dendritic cells from mice deficient in the leukotriene B4 receptor 1. *Biochimie.* 2010;92(6):682-691.
37. Kaech SM, Wherry EJ, Ahmed R. Effector and memory T-cell differentiation: implications for vaccine development. *Nat Rev Immunol.* 2002;2(4): 251-262.
38. Fearon DT, Manders P, Wagner SD. Arrested differentiation, the self-renewing memory lymphocyte, and vaccination. *Science.* 2001;293(5528): 248-250.
39. Kitajima M, Ito T, Tumes DJ, et al. Memory type 2 helper T cells induce long-lasting antitumor immunity by activating natural killer cells. *Cancer Res.* 2011;71(14):4790-4798.
40. Kryczek I, Banerjee M, Cheng P, et al. Phenotype, distribution, generation, and functional and clinical relevance of Th17 cells in the human tumor environments. *Blood.* 2009;114(6):1141-1149.
41. Muranski P, Restifo NP. Does IL-17 promote tumor growth? *Blood.* 2009;114(2):231-232.
42. Bronte V. Th17 and cancer: friends or foes? *Blood.* 2008;112(2):214.
43. Seder RA, Darrah PA, Roederer M. T-cell quality in memory and protection: implications for vaccine design. *Nat Rev Immunol.* 2008;8(4):247-258.
44. Gualde N, Cogny van Weydevelt F, Buffiere F, Jauberteau MO, Daculsi R, Vaillier D. Influence of LTB4 on CD4−, CD8− thymocytes: evidence that LTB4 plus IL-2 generate CD8+ suppressor thymocytes involved in tolerance to self. Effect of LTB4 and IL-2 on double negative thymocytes. *Thymus.* 1991;18(2):111-128.
45. Corthay A, Skovseth DK, Lundin KU, et al. Primary antitumor immune response mediated by CD4+ T cells. *Immunity.* 2005;22(3):371-383.
46. Qin Z, Blankenstein T. CD4+ T cell–mediated tumor rejection involves inhibition of angiogenesis that is dependent on IFN gamma receptor expression by nonhematopoietic cells. *Immunity.* 2000;12(6):677-686.
47. Yokomizo T, Kato K, Terawaki K, Izumi T, Shimizu T. A second leukotriene B(4) receptor, BLT2: a new therapeutic target in inflammation and immunological disorders. *J Exp Med.* 2000;192(3):421-432.
48. Okuno T, Iizuka Y, Okazaki H, Yokomizo T, Taguchi R, Shimizu T. 12(S)-Hydroxyheptadeca-5Z, 8E, 10E-trienoic acid is a natural ligand for leukotriene B4 receptor 2. *J Exp Med.* 2008;205(4):759-766.
49. Lin PY, Sun L, Thibodeaux SR, et al. B7-H1-dependent sex-related differences in tumor immunity and immunotherapy responses. *J Immunol.* 2010;185(5):2747-2753.
50. Scotland RS, Stables MJ, Madalli S, Watson P, Gilroy DW. Sex differences in resident immune cell phenotype underlie more efficient acute inflammatory responses in female mice. *Blood.* 2011;118(22):5918-5927.

Published OnlineFirst March 29, 2012; DOI: 10.1158/0008-5472.CAN-11-3185

Therapeutics, Targets, and Chemical Biology

Cancer Research

Coxsackievirus B3 Is an Oncolytic Virus with Immunostimulatory Properties That Is Active against Lung Adenocarcinoma

Shohei Miyamoto[1], Hiroyuki Inoue[1,2], Takafumi Nakamura[3], Meiko Yamada[4], Chika Sakamoto[1], Yasuo Urata[4], Toshihiko Okazaki[1], Tomotoshi Marumoto[1], Atsushi Takahashi[1], Koichi Takayama[2], Yoichi Nakanishi[2], Hiroyuki Shimizu[5], and Kenzaburo Tani[1]

Abstract

Although oncolytic virotherapy is a promising anticancer therapy, antitumor efficacy is hampered by low tumor selectivity. To identify a potent and selective oncolytic virotherapy, we carried out large-scale two-step screening of 28 enteroviral strains and found that coxsackievirus B3 (CVB3) possessed specific oncolytic activity against nine human non–small cell lung cancer (NSCLC) cell lines. CVB3-mediated cytotoxicity was positively correlated with the expression of the viral receptors, coxsackievirus and adenovirus receptor, and decay-accelerating factor, on NSCLC cells. *In vitro* assays revealed that the CVB3 induced apoptosis and phosphoinositide 3-kinase/Akt and mitogen-activated protein (MAP)/extracellular signal-regulated (ERK) kinase (MEK) survival signaling pathways, leading to cytotoxicity and regulation of CVB3 replication. Intratumoral injections of CVB3 elicited remarkable regression of preestablished NSCLC tumors *in vivo*. Furthermore, administrations of CVB3 into xenografts on the right flank resulted in significantly durable regression of uninjected xenografts on the left flank, where replication-competent CVB3 was detected. All treatments with CVB3 were well tolerated without treatment-related deaths. In addition, after CVB3 infection, NSCLC cells expressed abundant cell surface calreticulin and secreted ATP as well as translocated extranuclear high-mobility group box 1, which are required for immunogenic cell death. Moreover, intratumoral CVB3 administration markedly recruited natural killer cells and granulocytes, both of which contributed to the antitumor effects as shown by depletion assays, macrophages, and mature dendritic cells into tumor tissues. Together, our findings suggest that CVB3 is a potent and well-tolerated oncolytic agent with immunostimulatory properties active against both localized and metastatic NSCLC. *Cancer Res; 72(10); 2609–21. ©2012 AACR.*

Introduction

Oncolytic viruses are self-replicating, tumor-selective viruses, with an ability to directly induce cancer cell death, and have emerged as a promising treatment platform for cancer therapy (1).

Over the past 2 decades, clinical trials of oncolytic virotherapies using a range of DNA and RNA viruses including coxsackievirus A21 (CVA21), measles virus, Newcastle disease virus, and reovirus have been reported or are underway (2–5). Clinical development of these therapies has progressed to late phase trials. However, the antitumor efficacy of oncolytic viruses has yet to attain the potential anticipated in preclinical studies.

RNA viruses seem to be a safer modality, as most single-stranded RNA viruses replicate in the host cytosol without a DNA phase. Therefore, they lack the genotoxicity caused by integration of the viral genome into the host DNA. In particular, enteroviruses, members of the *Picornaviridae* family, a diverse group of small RNA viruses have emerged as promising candidates for cancer treatment (6–9). Their use has several therapeutic advantages: these viruses immediately induce robust cytolytic changes during cell-to-cell infection, they do not possess oncogenes that may lead to tumorigenesis, and they can be easily genetically manipulated by reverse genetics systems for the rescue of positive-strand RNA viruses from complementary DNA (10, 11). Furthermore, most nonpolio enteroviruses are common and highly prevalent and are mainly associated with asymptomatic infection or mild disease (12). Although CVA21 is reportedly a potent oncolytic enterovirus against

Authors' Affiliations: [1]Division of Molecular and Clinical Genetics, Medical Institute of Bioregulation; [2]Research Institute for Diseases of the Chest, Graduate School of Medical Sciences, Kyushu University, Fukuoka; [3]Core Facility for Therapeutic Vectors, The Institute of Medical Science, The University of Tokyo; [4]Oncolys BioPharma Inc.; and [5]Department of Virology II, National Institute of Infectious Diseases, Tokyo, Japan

Note: Supplementary data for this article are available at Cancer Research Online (http://cancerres.aacrjournals.org/).

S. Miyamoto and H. Inoue contributed equally to this work.

Corresponding Author: Kenzaburo Tani, Division of Molecular and Clinical Genetics, Medical Institute of Bioregulation, Kyushu University, 3-1-1 Maidashi, Higashi-ku, Fukuoka 812-8582, Japan. Phone: 81-92-642-6449; Fax: 81-92-642-6444; E-mail: taniken@bioreg.kyushu-u.ac.jp

doi: 10.1158/0008-5472.CAN-11-3185

Published OnlineFirst March 29, 2012; DOI: 10.1158/0008-5472.CAN-11-3185

miscellaneous human cancer cells (8, 9, 13), CVA21-treated mice died of lethal myositis with paralysis (14).

Apart from direct oncolysis, another important component of the sustained therapeutic advantage of oncolytic viruses depends on their ability to trigger antitumor immune responses (15). Robust viral replication in tumors provides immunologic damage-associated molecular pattern (DAMP) signals, augmenting the immunogenicity of the tumor microenvironment (16). Previous studies showed that several oncolytic viruses could induce adaptive antitumor immunity by tumor-specific CTL responses (17). However, little is known about how preceding innate immunity shapes the antitumor effects and whether oncolytic viruses cause immunogenic cancer cell death by similar mechanisms to chemotherapeutic agents, such as calreticulin (CRT) exposure, ATP release, or high-mobility group box 1 (HMGB1) translocation (18).

The focus of this study was to identify a novel oncolytic virus from screening 28 different strains of human enteroviruses, which had high tolerability when administered in mouse xenograft models, and to clarify the viral cytocidal mechanism by scrutinizing the apoptotic and antitumor immunogenic potential of the virus.

Materials and Methods

Mice

Female BALB/c nude mice were purchased from Charles River Japan. All animal experiments were carried out under the Guidelines for Animal Experiments of Kyushu University and Law 105 Notification 6 of the Japanese Government.

Cell lines

The non–small cell lung cancer (NSCLC; A549, H1299, and H460), colon cancer (Caco-2), pancreatic cancer (AsPC-1), renal cancer (A-498 and Caki-1), rhabdomyosarcoma (RD), T-cell leukemia (HuT 102), bone marrow stromal (HS-5), and normal lung fibroblast (MRC-5) cell lines were purchased from the American Type Culture Collection. NSCLC cell lines (PC-9, EBC-1, and LK-2) were obtained from the Health Science Research Resources Bank in Japan. Human lung squamous cell carcinoma cell lines (QG-56 and QG-95) were provided by Dr Y. Ichinose (National Kyushu Cancer Center; ref. 19). The other NSCLC cell lines (LK-87 and Sq-1) were obtained from Cell Resource Center for Biomedical Research, Tohoku University. Human cell lines of colon cancer (DLD-1), pancreatic cancer (PANC-1), breast cancer (MCF7), cervical cancer (HeLa S3), and normal lung fibroblast (NHLF) were provided by Dr T. Fujiwara (Okayama University). No authentication besides PCR tests that showed free from *Mycoplasma* contamination was done for all of cell lines used.

Production of enteroviruses

The 28 strains of enteroviruses tested were obtained from H. Shimizu (National Institute of Infectious Diseases, Japan) and were propagated in HeLa and RD cells. The $TCID_{50}$/mL on these cell monolayers was determined as previously described (20).

Crystal violet staining

Viable cells at 72-hour postinfection with enteroviruses at appropriate multiplicity of infection (MOI) for 1 hour were assessed by crystal violet staining as previously described (21). Cell survival rates were calculated by Multi Gauge software version 3.2 (FUJIFILM).

Flow cytometry analysis

Cells were incubated with a monoclonal antibody against coxsackievirus and adenovirus receptor (CAR; Upstate) followed by incubation with fluorescein isothiocyanate (FITC)-conjugated anti-mouse immunoglobulin G, or phycoerythrin (PE)-conjugated antibody decay-accelerating factor (DAF; BD Biosciences). For analysis of surface CRT, NSCLC cells infected with Coxsackievirus B3 (CVB3; MOI = 10) was analyzed by flow cytometric analysis (22). Data were obtained with a FACSCalibur (BD Biosciences) and analyzed by FlowJo software Version 7.6 (Tree Star Inc.).

MTS assay for cell viability

In vitro cell viability experiments using cells infected with CVB3 were carried out by a Cell Titer 96 AQueous Non-Radioactive Cell Proliferation Assay (Promega) following the manufacturer's instructions.

In vitro inhibition assays

Cells were pretreated with serum-free media containing the specific phosphoinositide 3-kinase (PI3K) inhibitor LY294002 (Santa Cruz Biotechnology), the PTEN inhibitor bisperoxovanadium (bpV, HOpic; Merck), or the mitogen-activated protein (MAP)/extracellular signal-regulated kinase (ERK; MEK) inhibitor PD0325901 (Wako) for 1 hour, and then infected with CVB3 (MOI = 10) for 1 hour. For apoptosis inhibition assay, A549 cells were pretreated with the pan-caspase inhibitor, z-VAD-fmk (100 or 200 μmol/L for 1 hour; R&D Systems), exposed to CVB3 at MOI of 0.01 or 0.1 for 1 hour, and replaced in indicated concentrations of z-VAD-fmk for additional 48 hours.

siRNA transfection assay

siRNAs specific for human CAR and a negative control were designed and synthesized by BONAC in Japan. Transfection of A549 cells with siRNAs was carried out with Lipofectamine 2000 (Invitrogen) according to the manufacturer's protocol. Following 72-hour incubation after transfection, cells were infected with CVB3 at MOI of 0.01 for MTS assays.

Western blot analysis

Cell lysate samples were resolved by SDS-PAGE and immunoblotted (21). The primary antibodies used were monoclonal antibodies against PARP (Biovision), phospho-Akt (Ser473; BioLegend), and β-actin (Santa Cruz Biotechnology). Densitometry analysis was conducted with LAS3000 (FUJIFILM) and Multi Gauge software version 3.2.

Annexin V staining and cell-cycle analysis

Apoptotic cells after CVB3 infection were determined with the Annexin V–PE apoptosis detection kit (BD Biosciences) according to the manufacturer's instructions. For cell-cycle

Published OnlineFirst March 29, 2012; DOI: 10.1158/0008-5472.CAN-11-3185

analysis, the cells were fixed in 70% ethanol, incubated with RNase A (50 μg/mL), stained with 10 μg/mL propidium iodide (PI), and analyzed with a FACS-Calibur.

ATP release assay

After cell death induction, secreted extracellular ATP was measured with the luciferin-based ENLITEN ATP Assay (Promega) according to the manufacturer's protocol.

Immunofluorescence microscopy

Cells fixed with 4% paraformaldehyde were permeabilized with 0.3% Triton X-100 for 10 minutes, incubated with anti-HMGB1 antibody for 30 minutes followed by incubation with Alexa Fluor 488–conjugated secondary antibody (Molecular Probes), and analyzed by a fluorescence microscope BZ-9000 (KEYENCE).

In vivo therapeutic studies

A549 cells (5×10^6 cells) or EBC-1 cells (3×10^6 cells) were injected subcutaneously into the right or bilateral flanks of nude mice. When tumors reached diameters of 0.4 to 0.6 cm, the tumors on the right flank were inoculated with CVB3 (5×10^6 $TCID_{50}$) once on day 2 or with the same doses of CVB3 on days 2, 4, 6, 8, and 10.

The RB6-8C5 rat hybridoma cell line producing the anti-mouse Gr-1 monoclonal antibody was provided by Dr T. Yokomizo (Kyushu University). For granulocyte depletion, nude mice implanted with 5×10^6 A549 cells were intraperitoneally injected with 300 μg rat anti–Gr-1 antibody (99.7% elimination of circulating polymorphonuclear neutrophils). For natural killer (NK) cell depletion, nude mice were intraperitoneally injected with rabbit polyclonal anti-asialo GM1 antibody (Wako; ref. 23). The tumor volume was calculated as length × width × width/2 and expressed as means ± SEM. Animals were euthanized when the tumor diameter exceeded 1.0 cm.

Tumor-infiltrating lymphocytes

The excised tumors were gently homogenized with sharp syringes, incubated for 90 minutes in RPMI-1640 containing collagenase (Invitrogen). For innate immunity subpopulations, the cells were stained with anti-mouse DX-5-FITC, Gr-1-PE, F4/80-APC, or CD11c-APC antibodies for 30 minutes. For mature dendritic cells (DC), the cells were stained with anti-mouse CD86-FITC, CD80-PE, CCR7-PerCP, and CD11c-APC antibody for 30 minutes. For cytolytic effector cells, the cells were stained with anti-mouse DX-5-FITC, Gr-1-PerCP, and CD107a-PE antibody for 30 minutes (24) and analyzed by a FACS Calibur.

Statistical analyses

Statistical analyses were conducted with GraphPad Prism 5.0d software package (GraphPad Software Inc.). Statistical analysis was conducted using a 2-tailed unpaired Student *t* test, one-way ANOVA followed by Tukey multiple comparison test, or nonparametric Mann–Whitney *U* test. $P < 0.05$ was considered statistically significant. Survival curves were plotted according to the Kaplan–Meier method (log-rank test).

Results

Sequential two-step screening identifies CVB3 as a candidate for oncolytic virus against NSCLC

To identify a safer and more potent oncolytic enterovirus, we carried out a large-scale screening of 28 strains of enteroviruses for oncolytic activity. This screening was carried out *in vitro* against 12 different human cancer cell lines and the HS-5 normal bone marrow stromal cell line using crystal violet staining. Several enteroviruses displayed marked cytotoxic effects (Fig. 1A) in a dose-dependent manner (Supplementary Fig. S1A and S1B). The Coxsackievirus B group, CVB2 (Ohio-1), CVB3 (Nancy), and CVB4 (J.V.B.) were of particular interest, as they showed exclusive oncolytic effects on the A549 and LK-87 NSCLC cell lines (Fig. 1A). In a secondary screen, we evaluated the oncolytic efficacy of CVB2, CVB3, and CVB4 against 9 additional NSCLC cell lines and 2 normal lung cell lines. Unexpectedly, only CVB3 infection induced marked cytolysis in 100% (9 of 9) NSCLC cell lines of diverse histologic subtypes, that is, adenocarcinoma (A549), squamous cell carcinoma (EBC-1), and large cell carcinoma (H460) even at an MOI of 0.001. However, CVB3 did not induce cytolysis against normal lung fibroblast cell lines even at an MOI as high as 10 (Fig. 1B). Accordingly, we employed CVB3 harboring potent and specific cytolytic activity as a candidate virus for oncolytic virotherapy against NSCLC.

Correlation of CVB3-mediated cytotoxicity and expression levels of surface receptors on NSCLC Cells

We next compared the expression level of the CVB3 receptors, CAR and DAF (25) on various human NSCLC and normal lung cell lines. NSCLC cell lines expressed moderate to high levels of CAR, whereas normal lung cell lines expressed very low levels of CAR. The expression of DAF was similarly high in the NSCLC and normal lung cell lines (Fig. 2A). The oncolytic activity of CVB3 significantly correlated with a number that was equal to the percentage of CAR-expressing cells multiplied by the percentage of DAF-expressing cells ($r = -0.92$, $P < 0.0001$), whereas 2 normal lung cell lines were unaffected (Fig. 2B). The results of the *in vitro* MTS cell viability assays confirmed this correlation in a time-dependent manner (Fig. 2C). To thereby elucidate the role of CAR in the cytolytic effects of CVB3, CVB3-infected A549 cells were analyzed in the presence of siRNA-mediated functional CAR knockdown. Flow cytometric analyses confirmed the reduction of CAR expression by 92% in A549 cells transfected with CAR-specific siRNA (Supplementary Fig. S2). The inhibition of CAR significantly abrogated the cytotoxicity of CVB3 ($P < 0.001$; Fig. 2D).

Contribution of caspase-mediated apoptosis and PI3K/Akt or MEK/ERK signaling pathways to CVB3-mediated cytotoxicity in NSCLC cells

To determine whether CVB3 induced apoptosis in NSCLC cells treated with CVB3 (MOI = 0.1), we examined the cleavage of PARP by caspases, an execution marker of apoptosis. Western blot analysis revealed cleaved PARP (85 kDa) in CVB3-treated A549 and LK-2 NSCLC cells, but not in CVB3-

Published OnlineFirst March 29, 2012; DOI: 10.1158/0008-5472.CAN-11-3185

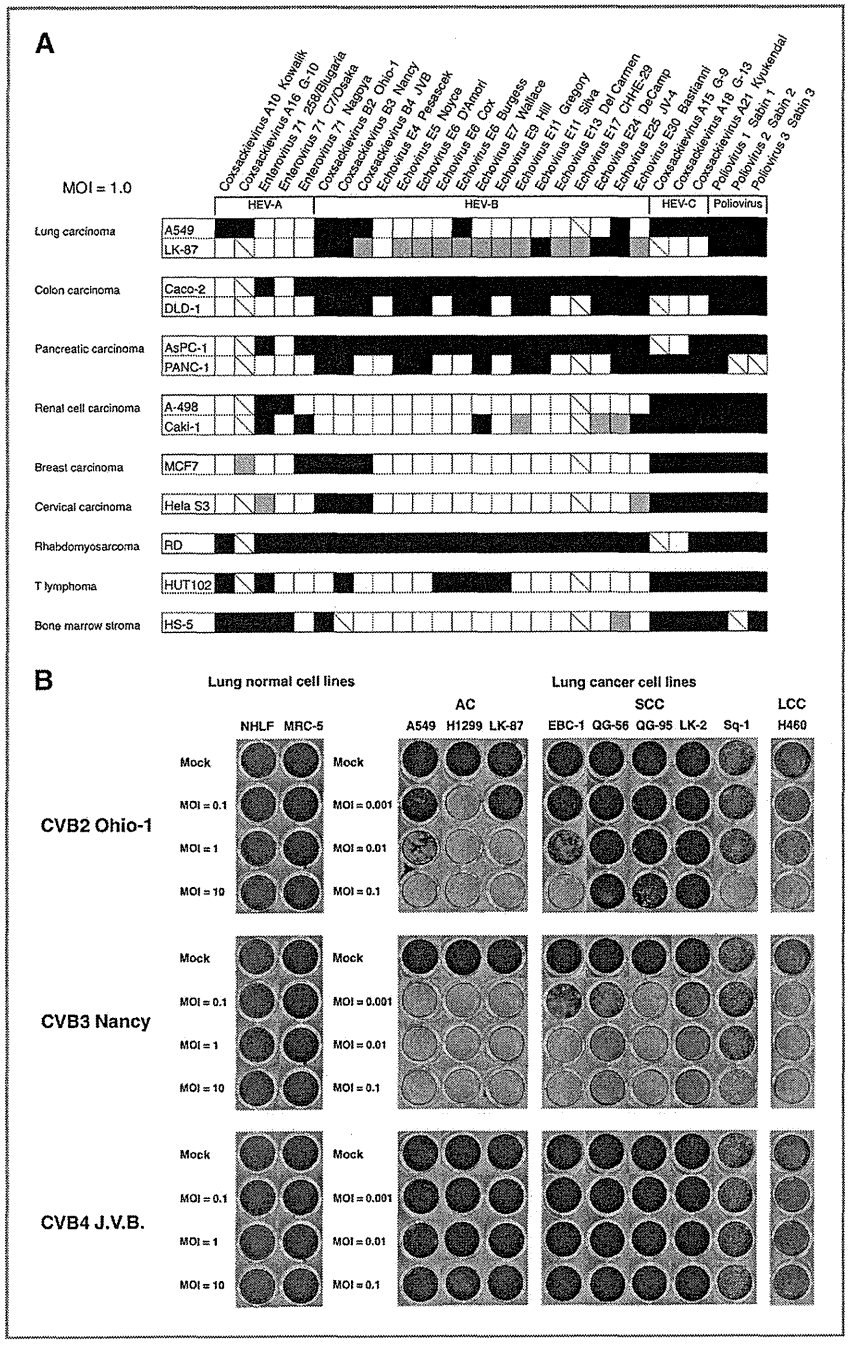

Figure 1. Sequential 2-step screenings to identify a potent oncolytic virus candidate. A, various cancer cell lines and HS-5 cells were infected with 28 strains of enterovirus at an MOI of 1.0 and incubated for 1 hour. At 72 hours postinfection, cell viability was assessed by crystal violet staining. Black, gray, white, and hashed boxes indicate greater than 50% cytotoxicity, less than 50% cytotoxicity, no cytotoxicity, and not analyzed, respectively. HEV-A, human enterovirus A; HEV-B, human enterovirus B; HEV-C, human enterovirus C. B, various human NSCLC and normal lung cell lines were infected with CVB2, CVB3, and CVB4 for 72 hours at MOIs of 0.001, 0.01, and 0.1 for NSCLC cell lines and MOIs of 0.1, 1.0, and 10 for normal cell lines, respectively. Cell viability was assessed by crystal violet staining. AC, adenocarcinoma; SCC, squamous cell carcinoma; LCC, large cell carcinoma.

treated MRC-5 normal lung cells (Fig. 3A). We analyzed externalization of phosphatidylserine and DNA fragmentation, hallmarks of apoptosis. CVB3-treated A549 cells showed a greater proportion of apoptotic (AnnexinV$^+$/7-AAD$^-$) and necrotic (AnnexinV$^+$/7-AAD$^+$) cells than LK-2 cells, correlating with CAR expression (Fig. 3B). Similarly, exposure of A549 cells to CVB3 induced more sub-G_1 cells with DNA fragmentation than LK-2 cells, correlating with CAR expression. In contrast, neither Annexin V positivity nor DNA fragmentation was induced in CVB3-treated MRC-5 cells (Fig. 3C). To determine whether

Published OnlineFirst March 29, 2012; DOI: 10.1158/0008-5472.CAN-11-3185

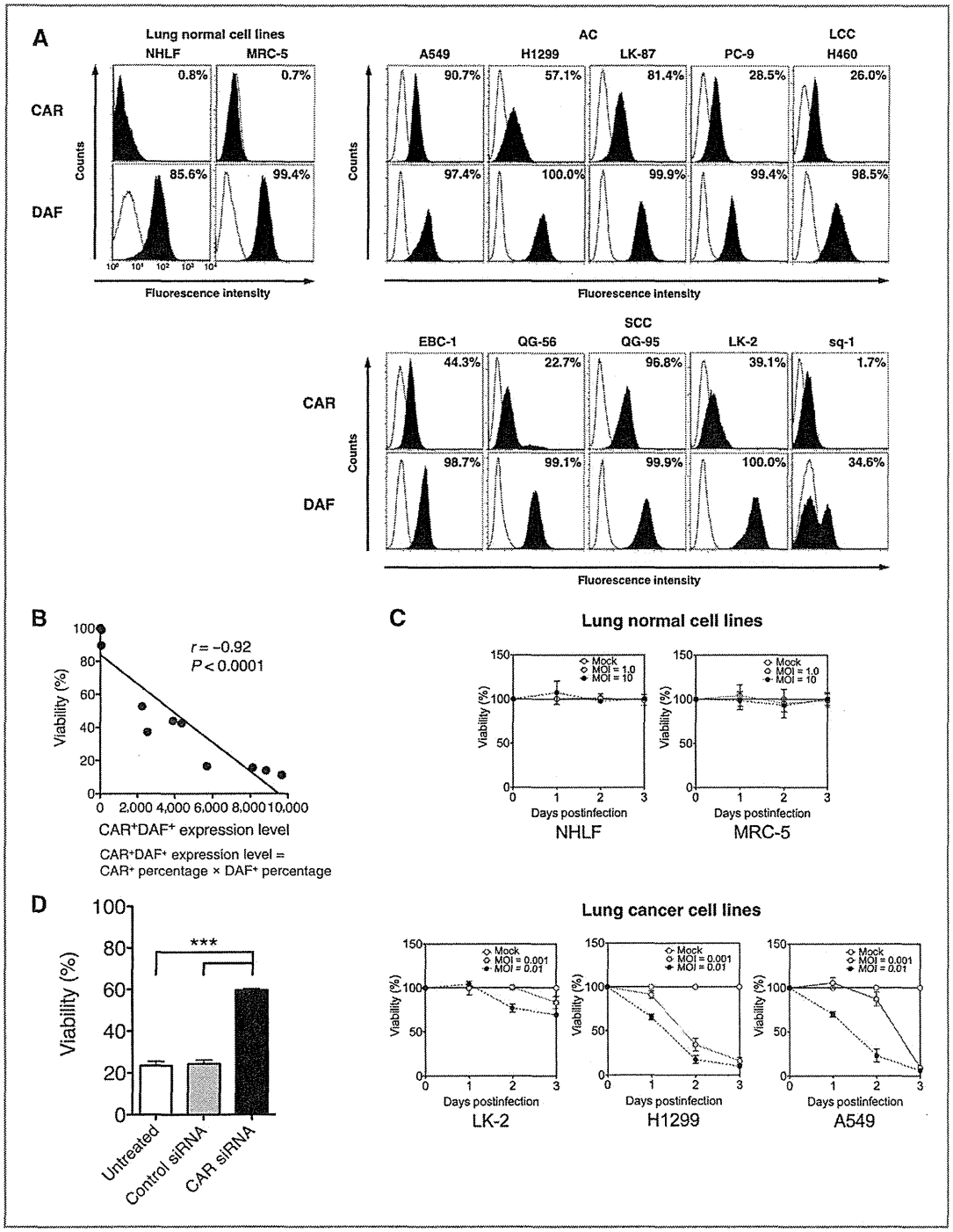

Figure 2. Expression profile of surface CAR and DAF on normal lung and NSCLC cells and its correlation with CVB3-mediated cytotoxicity. A, surface expression of CVB3 receptors on various lung cell lines was quantified by flow cytometry. Histograms represent the measured fluorescence of cells incubated with an isotype control antibody (unshaded) and anti-CAR or anti-DAF antibody (shaded). B, correlation between expression of CAR and DAF and cell viability at 72 hours after CVB3 infection ($r = -0.92$; $P < 0.0001$). C, cells infected with CVB3 at indicated MOIs was analyzed at indicated time points for cell viability by MTS assay. Each value was normalized to Opti-MEM–treated cells (mock) and represents the mean ± SD. D, A549 cells transfected with CAR-specific siRNA or control siRNA were infected with CVB3 (MOI = 10), and assessed by MTS cell viability assay at 48 hours after CVB3 infection. Each value was normalized to mock and represents the mean ± SD. ***, $P < 0.001$.